NRL Report 5920

Fracture Analysis Diagram Procedures for the Fracture-Safe Engineering Design of Steel Structures

W. S. Pellini and P. P. Puzak
Metallurgy Division

March 15, 1963

APPROVED FOR PUBLIC RELEASE - DISTRIBUTION UNLIMITED

U.S. NAVAL RESEARCH LABORATORY
Washington, D.C.

CONTENTS

INTRODUCTION 1

CONCEPT OF THE FRACTURE ANALYSIS DIAGRAM 1

EXPERIMENTAL BASIS FOR THE LOCATION OF THE CAT CURVE 8

EXPERIMENTAL BASIS FOR THE LOCATION OF THE FRACTURE INITIATION CURVES 10

RESIDUAL STRESS RELATIONSHIPS TO THE FRACTURE ANALYSIS DIAGRAM 11

VALIDATION OF THE FRACTURE ANALYSIS DIAGRAM – SERVICE FAILURES AND PRESSURE VESSEL TESTS 13

Category A: Temperature Below NDT – Plastic Strain Loading of Small Flaws 14

Category B: Temperature Below NDT – High-Level, Residual Stress Loading of Small Flaws 19

Category C: Temperature Below NDT – Elastic Stress Loading of Large Flaws 35

Category D: Temperature Between NDT and CAT Curve – Elastic Stress Loading of Large Flaws 39

Category E: Temperature at FTE – Plastic Strain Loading of Moderately Large Flaws 40

Category F: Temperature Above FTE and Above FTP – Near Ultimate Tensile Strength Loading of Very Large Flaws 46

GENERAL PROCEDURE FOR THE FRACTURE-SAFE ENGINEERING USE OF STEELS BASED ON THE FRACTURE ANALYSIS DIAGRAM 50

ACKNOWLEDGMENTS 52

REFERENCES 52

SELECTED BIBLIOGRAPHY RELATING TO THE DEVELOPMENT AND APPLICATIONS OF THE DROP-WEIGHT TEST 53

Copies available from the Office of Technical Services,
Department of Commerce - $1.50

Fracture Analysis Diagram Procedures for the Fracture-Safe Engineering Design of Steel Structures

W. S. PELLINI AND P. P. PUZAK
Metallurgy Division

A new procedure is described for the engineering design of fracture-safe steel structures representing weldments, forgings, castings, and combinations of these. The procedure is applicable to all steels which have distinct transition temperature features, *i.e.*, excepting the ultrahigh strength types which have poorly defined, low-slope Charpy V transition curves. The new procedure is based on the concept of the fracture analysis diagram, which represents a consolidation of the available knowledge concerning flaw size, stress, and temperature requirements for the initiation and propagation of brittle fractures. The bases for the development of the diagram are explained. Extensive failure and structural test data are provided as documentation of the validity of the described procedures. The practical engineering use of the fracture analysis diagram is based on the determination of a simple parameter – the NDT temperature of the steel. All other required information involves elements which are normal considerations in design of engineering structures.

INTRODUCTION

Those who have a "users" interest in the fracture literature will find that many of the papers on the subject cover too narrow a span of interest to be useful for the solution of practical problems. Attempts by lay readers to integrate the available fund of knowledge have floundered on the sheer impossibility of coping with a mass of apparently contradictory information.

This report is presented as a summary of the status of integration of available knowledge, attained by the authors as the result of almost 15 years of concentrated research effort and detailed study of the literature in the field. During this period, the objective of developing a practical engineering approach to the fracture problem was a matter of considerable urgency due to a steady succession of service failures, many of which required immediate solutions and the acceptance of responsibility for the solutions. In many cases the solutions were provided with the clear knowledge that military objectives, life, and property values in terms of millions of dollars hinged on the decisions. Such items, which rarely creep into formal technical publications, are worthy of note to highlight the "firing line" atmosphere which provided the impetus to analyze all available information to the limit. Except for this atmosphere, this report would not have been written.

The confidence which was developed during this long period of test and retest of concepts, is now expressed in the presentation of a detailed "package approach" to the engineering problem of fracture-safe design. The approach covers intermediate- and low-strength steels, commonly referenced as the structural grades, in the form of plates, forgings, weldments, castings and combinations of these. The elements of this package include: (a) practical testing procedures suitable to anybody's laboratory, (b) simplicity of an analysis which is understandable to the general engineering field, (c) flexibility in application to a wide gamut of engineering structures – from 5/8-in.-thick plate weldments to castings and forgings of thickness measured in terms of feet, (d) extensive documentation with respect to a wide range of service failures and simulated service tests and (e) an extensive background of successful applications of the test procedures to a wide range of structures in present service to serve as a basis for confidence.

Despite the length of this report, it unfortunately remains as a severe abridgement of the total approach package developed by the authors. The intent is to provide a base-line presentation, which will make future discussions of more detailed aspects understandable within a framework of basic reference.

CONCEPT OF THE FRACTURE ANALYSIS DIAGRAM

Brittle fractures are characterized by the propagation of cracks at velocities of several thousand feet per second. The fractures are observed to be normal to wall surfaces (square-break) and of crystalline texture, indicating that the individual grains of the steel fractured by cleavage of crystal planes. In general, there is very little visible evidence of plastic flow, except for thin fins or

NRL Problem M01-01; Projects SR 007-01-01 (Tasks 0854 and 0850) and RR-007-01-46-5414. This is a final report on one phase of this problem; work on other phases of the problem is continuing.

"shear lips" at the free surfaces of the crack. In contrast, ductile fractures show a 45-degree shear tear involving severe plastic deformation of the individual grains; in effect, the "shear lip" covers the entire fracture surface. Except for certain types of ultrahigh strength steels, and nonferrous alloys, the 45-degree shear fractures develop only by the application of gross plastic overloads approaching the ultimate tensile strength of the steel. The propagation of such fractures proceeds only at the rates of continued reapplication of the plastic overloads and therefore with very high absorption energy. Brittle fractures, on the other hand, are propagated in a manner which may be described as "spontaneous" in that the small amount of required driving energy is entirely derived from the release of elastic strain energy.

Brittle fractures may be initiated at conventional design levels of nominal elastic stress, provided certain other conditions are satisfied, as follows: (a) a flaw such as a crack or sharp notch is present, (b) the stress is of sufficient intensity to develop a small amount of deformation at the notch tip, and (c) the service temperature is low enough to promote cleavage fracture of the deformed metal crystals at the notch tip.

In other words, the initiation of fracture at nominal elastic load levels is determined by the cleavage cracking tendencies of a small volume of steel at notch tips. If "crackless" plastic flow occurs at the notch tip, the structure is not endangered because a surrounding larger volume of metal readily assumes the burden of supporting the stress. If cleavage cracking occurs, a sharp natural crack front is extended into the metal by a high-speed repetition of the crack tip cleavage process, resulting in a "propagation" of the brittle fracture.

With decreasing temperatures, the transition from ductile behavior at crack tips to cleavage behavior is developed "sharply" in a narrow temperature range. The "sharpness" of the transition provides the basis for what is generally termed the transition temperature approach to the fracture problem. In the prior use of the transition temperature approach, the basic problem has been that flaw size and stress factors were not interpretable. That is to say, the transition temperature approach was based simply on correlations of certain levels of notch bar fracture toughness that appeared to separate corresponding service temperatures of failure from those of no failure, namely, Charpy V correlations for fractured ships. The fracture analysis diagram approach was developed from concepts evolved by the senior author (W.S.P.) in 1961 – these concepts involving a meshing of fracture mechanics flaw size and stress factors with the transition temperature test approach. By combining the best features of the two approaches, there emerged the first practical, analytical method for the engineering design of fracture-safe structures.

The design method is based on a generalized stress-temperature diagram for fracture initiation and crack arrest. This diagram may be related to the service temperature by determination of one of several significant reference transition temperatures. A simple method for determining a reference transition temperature is provided by the drop-weight test or by the Charpy-V test as correlated with the drop-weight test. This reference temperature is designated as the nil ductility transition temperature – NDT temperature (1,2).

The significance of the NDT temperature may be brought out by discussion of the general effects of temperature on the fracture stress transition of steels (Fig. 1). A flaw-free steel is illustrated to develop a gradually increasing tensile strength (T.S.) and yield strength (Y.S.) with decreasing temperature; the increase in yield strength is greater than that of the tensile strength, resulting in coincidence at some very low temperature. At the temperature of coincidence, tensile ductility as measured by elongation or reduction of area (plastic flow) is decreased to essentially zero or nil value. This temperature may be considered as the NDT temperature in the *absence* of a flaw. If a small, sharp flaw is placed in the test specimen, such as a plate, a decreased level of fracture stress is obtained in the transition range as indicated by the dashed curve labeled "fracture stress decrease due to small, sharp flaw." The highest temperature at which the decreasing fracture stress for fracture initiation due to the small flaw becomes contiguous with the yield strength curve of the steel is defined as the nil ductility transition (NDT) temperature. Below the NDT temperature the fracture stress curve for the small flaw follows the course of the yield strength curve, as indicated by the continuation of the dashed curve to lower temperatures. The arrows pointing down from the NDT point indicate that increases in the flaw size result in progressive lowering of the fracture stress curve to lower levels of nominal stress. As an approximation, the fracture stress is inversely proportional to the square root of the flaw size. The resulting family of fracture stress curves are characterized by a common temperature effect, involving a marked increase in the stress required for fracture as the temperature is increased above the NDT temperature.

A curve noted as CAT (crack arrest temperature) is drawn to represent the fracture *arrest* relationship between stress and temperature. The CAT curve represents the temperature of arrest of a propagating brittle fracture for various levels of applied nominal

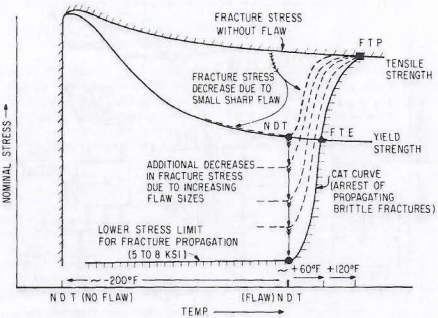

Fig. 1 — Transition temperature features of steels

stress. The crack arrest temperature for a stress level equal to the yield strength has been defined by the authors in previous reports as the "fracture transition elastic" (FTE) temperature and marks the highest temperature of fracture propagation for purely elastic loads. Similarly, the "fracture transition plastic" (FTP) temperature has been defined as the temperature above which fractures are entirely shear, *i.e.*, show no center regions of cleavage fracture, and the stress required for fracture approximates the tensile strength of the steel. The lower shelf in the range of 5 to 8 ksi, labeled as the "lower stress limit for fracture propagation" represents the stress level, below which fracture propagation is not possible because the minimum, small amount of elastic strain energy release required for continued propagation of brittle fractures is not attained.

The various types of tests which have provided data required to chart this diagram are illustrated in Fig. 2. Crack arrest tests may be conducted with a composite plate comprising a brittle plate welded to a "test" plate, sketch (A). After the assembly is brought to a specific temperature and stress level, "forced" initiation of a fracture in the brittle plate by wedge impact is used to develop a rapidly running brittle fracture. The fracture continues through the "test" steel or stops, depending on whether the temperature is below or above the CAT for the steel at the specific stress level of the test. A series of tests are conducted to establish the boundary of the "run" and "stop" temperatures. Variations of this test include wedge impact starting of a fracture in the test plate itself, sketch (B), or in a prolongation of the test plate, which is cooled to low temperatures. Data on crack arrest properties at stresses and temperatures above the FTE point have been obtained primarily by the use of crack-starter explosion tests, sketches (C) and (D), to be explained. FTP performance in this test is indicated by the development of a deep hemispherical bulge with fractures restricted to short, shear tears, sketch (D).

Large-scale, fracture initiation tests have been conducted by introducing flaws (fatigue cracks, brittle weld cracks, etc.) of various dimensions in a test plate and loading to establish the fracture stress, sketches (E) and (F). Figures 1 and 2 illustrate that the family of dashed curves representing the fracture initiation stress for various flaw sizes are bounded or "cut off" by the CAT curve. This curve begins to rise sharply at the NDT temperature with a slope such that the CAT for yield stress loading (FTE) is reached at NDT + 60°F and FTP properties are reached at NDT + 120°F.

The importance of the NDT temperature *as a reference point for the generalized diagram* resides in the fact that it may be determined easily by the use of the drop-weight test. Figure 3 illustrates a drop-weight test specimen before and after test below the NDT temperature. The drop-weight test features the use of a brittle weld bead which cracks on "bend" loading to the yield point of the test plate surface. The resulting brittle crack represents the starting flaw or notch. The size of this

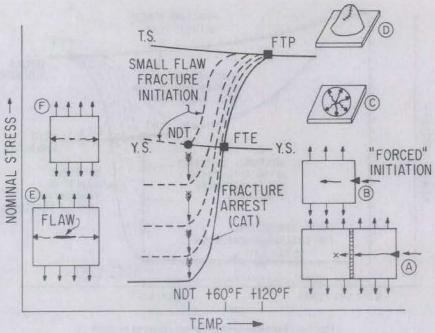

Fig. 2 – Features of large-scale fracture initiation and fracture arrest tests

flaw (approximately 1/2 × 1/4 in.) characterizes the test as a "small flaw" initiation test. A stop placed beneath the center point of the specimen span restricts the test loading to stress conditions involving incipient yielding. The specimen shown represents the smallest size of a series of sizes that may be used (1,2). Figure 4 illustrates the simplicity of the test equipment; details of the anvil are evident from the enlargement. The samples are brought to a desired temperature, placed on the test anvil, and the weight released to provide for loading to the point controlled by the stop. As illustrated by Fig. 5, a series of specimens are tested at 10°F intervals – the highest temperature of "break" indicates the NDT of the steel. The sharp transition from "break" to "no break" at the NDT temperature results from the marked increase in the levels of deformation required for fracture initiation at temperatures above the NDT. This feature is illustrated by the steep slope of the fracture stress curve which corresponds to "small flaw" condition of the drop-weight test at temperatures above the NDT point, Figs. 1 and 2.

Figure 6 documents the high resistance to fracture initiation exhibited by the same steel shown in Fig. 5 for tests at temperatures above the NDT, with a special demonstration series featuring an open span (no stop). Unlike most laboratory fracture tests which tend to develop data scatter, the drop-weight test is highly reproducible. Another feature of the test is that it is insensitive to orientation with respect to rolling or forging direction. This is due to the fact that a small-flaw test specimen can break only at a temperature of complete brittleness and brittle fractures are insensitive to orientation. Thus, a steel is characterized by a single NDT and problems of orientation definition are eliminated.

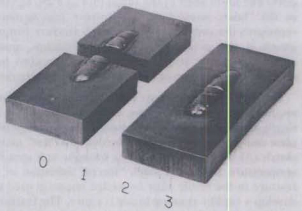

Fig. 3 – Drop-weight test specimen (2×5×5/8 in.) before test (right) and after test at, or below, the NDT temperature (left), illustrating the function of the brittle weld as a "crack starter" flaw

The dramatic change in fracture toughness of steels over a relatively narrow temperature range is best illustrated by explosion crack-starter tests. In this test, plates containing the brittle crack-starter weld (thus—a small flaw condition) are explosion loaded while placed over a circular die. An explosive wafer is placed approximately 1-1/2 ft above the test plate so as to develop gas pressure loading rather than a spalling type contact loading. In the absence of the crack-starter weld, the plates would develop a hemispherical bulge with a flat rim, representing the edge regions of explosive "hold down" against the die support face.

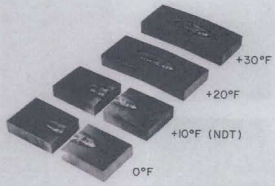

Fig. 5 —Typical drop-weight test series, illustrating an NDT at 10°F

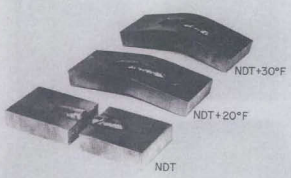

Fig. 6 — Open anvil test series illustrating bend deformation (ductility) developed at temperatures above the NDT temperature as compared to the "flat break" at and below the NDT temperature

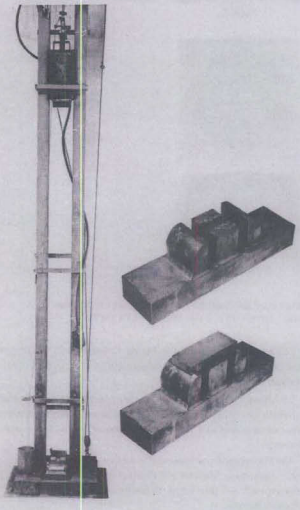

Fig. 4 — Drop-weight test equipment (left); details of anvil for 2×5×5/8 in. specimens (right)

Figure 7 presents a panoramic view of the dramatic temperature effect in 20°F steps, for a World War II ship plate steel test series. At and below the NDT temperature, 20°F for this steel, the test plates break "flat." Above the NDT temperature the plates *bulge* before fracture, indicating difficult (plastic strain required) starting of the fracture. In conformance with the plastic strain-temperature relationships of the small flaw fracture initiation curve at temperatures above the NDT temperature, the level of pre-fracture bulging (plastic stress levels) increases continuously with increasing temperature in the NDT to FTP range. The fractures, once started, run through the "hold down" regions of the bulge (elastically loaded die supported regions) at all temperatures below the FTE. At temperatures above the FTE, the fractures are entirely contained in the

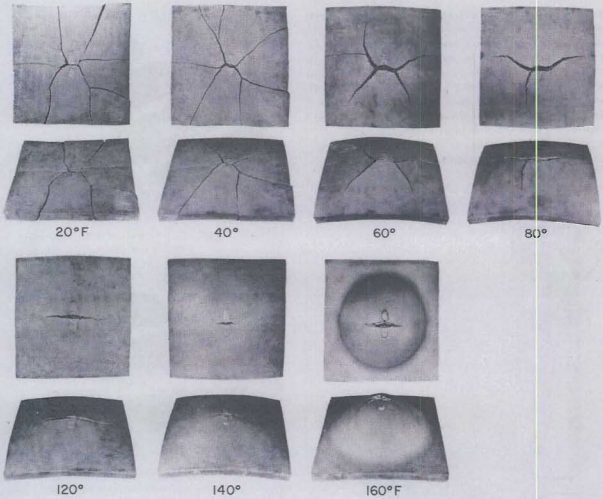

Fig. 7 — Explosion crack-starter test series in 20°F steps illustrating the dramatic increase in fracture toughness of steels above the NDT temperature (for the steel shown, NDT = 20°F, FTE = 70°F, and FTP = 140°F)

plastic loaded regions of the bulge (short fractures). Above the FTP temperature only short, ductile tears are developed, even with the intentional forcing of deformation to a complete hemisphere, as shown by the 160°F test plate of the series. The FTP temperature is approximately 120°F above the NDT temperature. These results have been confirmed for a wide variety of steels and for plates up to 3 in. in thickness.

By reference to Fig. 8, we may now relate drop-weight and explosion test performance to the fracture analysis diagram, as follows:

1. Nil ductility (fracture of drop-weight specimens and flat break in explosion tests) occurs at and below the NDT temperatures.

2. Levels of prefracture bulge deformation increase as test temperatures are raised above the NDT temperatures.

3. Above the FTE temperature, fractures do not run through the elastic load or "hold down" regions, thus indicating the CAT for yield stress loading has been exceeded.

4. Propagation of partially brittle fractures through the plastically deformed center regions of bulge are developed in the range between the FTE and FTP temperatures.

5. Short, shear tears are developed above the FTP temperature. The use of unusually large amounts of explosives results in the development of a deep bulge.

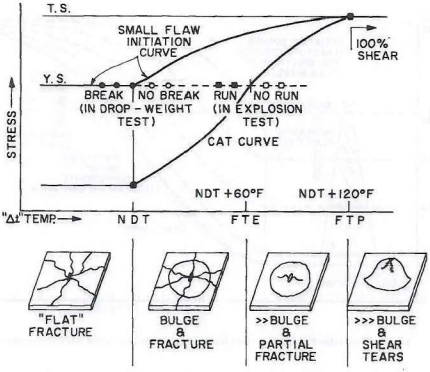

Fig. 8 – Drop-weight and explosion crack-starter test series related to the generalized fracture diagram

The observed increase in fracture toughness with increasing temperature is characterized by the gradual transition of the fracture surfaces from a completely brittle fracture, except for very thin (visible with magnification) shear lips at and below the NDT, to heavy shear lips (1/8 in.) at FTE, and to full shear at and above the FTP. These various observations were first made during a period of extensive testing of a wide variety of plate steels in 1950–1953. The terminology and interpretation of NDT, FTE, and FTP, which was developed during this early period remains valid; however, a more exact definition of the nature of the events is now possible based on crack arrest data and "flaw size" fracture stress data developed by other investigators.

The approximate range of flaw sizes required for fracture initiation at various levels of nominal stress are illustrated by the generalized fracture analysis diagram of Fig. 9. The flaw size data have been derived from a wide variety of small flaw tests, from limited studies of tensile tests with large flaws introduced into 1 in. and 3/4 in. thick plates, and from theoretical fracture mechanics concepts developed by G. R. Irwin (3). Validation is provided by a large amount of failure and structural test data, to be presented. The generalized diagram presents a family of fracture initiation curves relating to a range of flaw sizes. These range from flaws of less than 1 in. (top dashed curve) to flaws in the order of 1 to 2 ft (bottom dashed curve). It should be noted that all initiation curves have been drawn to show a rapidly increasing requirement for higher stresses with increasing temperature above the NDT temperature. The actual slope and shape of the "rising" portions of the initiation curves represent estimates based on the general slope of the crack arrest curve.

The diagram predicts that for a given level of stress, larger flaw sizes will be required for fracture initiation above the NDT temperature. For example, at stresses in the order of 3/4 Y.S., a flaw in the order of 8 to 10 in. may be sufficient to initiate fracture below the NDT temperature; however, at NDT + 30°F, a flaw of 1-1/2 to 2 times this size may be required for initiation. To the right of the CAT, there is "no flaw" that is of sufficient size to initiate fracture because propagation of brittle fractures is not possible. It should be noted that the nominal stress plotted in this diagram is the stress acting on the volume of material within which the flaw resides. Thus, for a flaw residing in the shell region of a pressure vessel, the nominal stress is the shell stress vector component; for a flaw residing at a nozzle the nominal stress is the higher level of stress acting at that particular position in the nozzle.

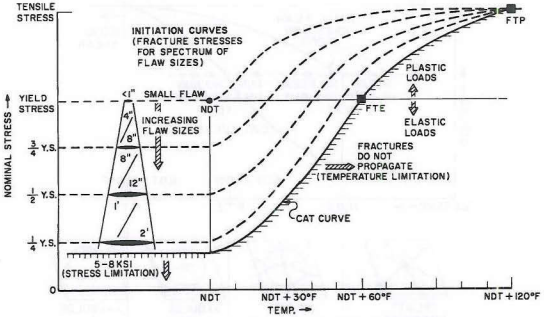

Fig. 9 — Generalized fracture analysis diagram, as referenced by the NDT temperature

EXPERIMENTAL BASIS FOR THE LOCATION OF THE CAT CURVE

We shall first discuss the basis for the shape of the CAT curve and of its position with respect to the NDT temperature. The basis is found in a compilation of all available crack arrest data for steel plates that also had been tested with the drop-weight test to establish the NDT temperature. Figure 10 illustrates a typical correlation of NDT and CAT data resulting from tests conducted by Mosborg (4). A series of combination plates comprising a 3/4-in.-thick ABS-C test plate of 5-ft width welded to a 1-ft-wide "crack-starter" plate provided the necessary specimens. These assemblies were loaded to stress levels in the order of 1/2 the yield strength of the test steel and a hammer blow was applied to a wedge inserted in a notch located at the edge of the brittle "crack-starter" plate. A brittle fracture was thereby initiated which propagated across the starter plate and either stopped on entering the test plate or continued through to complete fracture, depending on the test temperature. The data presented in Fig. 10 illustrate a sharp cutoff in fracture propagation at temperatures in the range of 30° to 35°F above the NDT temperatures of the three plates from the same heat which were used to fabricate the specimens. At temperatures below the indicated CAT curve, all tests resulted in complete fracture, while at higher temperatures the fracture stopped on *entering* the test plate.

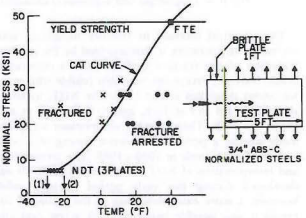

Fig. 10 — Correlation of CAT data obtained by Mosborg (4) with NDT temperatures of the test steels. The data relate to three separate plates from one heat.

A summary of Esso brittle temperature (EBT) crack arrest data for a wide variety of 3/4 to 1 in. structural steel plates is provided in Fig. 11. The EBT test differs from the Mosborg type test in that the brittle "starter" plate is not used, fracture initiation is obtained in the test plate by the application of a local "overstress," due to the wedge action. The test plate width is ordinarily in the order of 16 in.; however, tests also have been conducted for 6-ft-wide plates. The EBT tests were conducted at the 18-ksi stress level, *i.e.*, at approximately 1/2

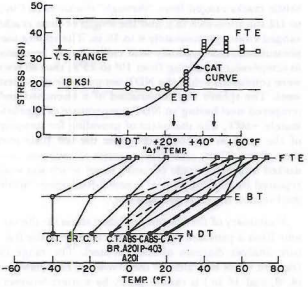

Fig. 11 – The lower graph illustrates the temperatures determined for the NDT, EBT, and FTE for 12 steels; the data relating to each steel are connected by a reference line. The "Δt" relationships of the EBT and the FTE to the NDT temperature are summarized in the upper graph. The crack arrest curve drawn in the top graph represents the "mean position" CAT curve indicated by the "Δt" data points.

the yield strength of the test steels. These steels are commonly used in the fabrication of large storage tanks in this country and in England—full details are available from Ref. 5. The NDT and FTE tests were conducted by the authors using material provided by the Esso authors.

The lower graph provides the individual data points for each steel. The diagram at the top of the figure summarizes the "Δt" temperature relationship of the EBT and FTE temperatures to the NDT temperatures. The EBT crack arrest point for the 18-ksi stress level as defined by these tests appears to have a mean position of 25°F above the NDT. The FTE crack arrest point for the yield stress level has a mean position of 45°F above the NDT.

A similar summary of all available correlation data is presented in Fig. 12. These include the data presented in Figs. 10 and 11 plus the results obtained for other steels (6) using the isothermal (T_K) Robertson, 3 ft "brittle" plus 3 ft "test" composite plates, and 6-ft test plates. Except for the FTE explosion tests, all data are for stress levels approximating 1/2 the yield strength of the test steels. Based on a "high end" of the correlation range, the CAT point is defined as 30°F above the NDT temperature for stress levels in the order of 1/2 the yield strength and 60°F above the NDT for stress levels in the order of the yield strength. There are two limitations to

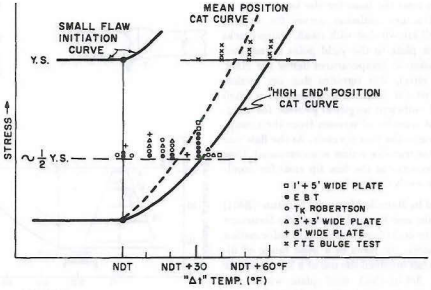

Fig. 12 – Summarization of "Δt" CAT data for 32 steels, representing a wide variety of tests conducted at stress levels of approximately 1/2 the yield strength level of the various steels. A total of 14 steels were also tested by the explosion crack starter test to establish the "Δt" FTE (CAT for Y.S. level). These data represent the bases for the fracture analysis diagram location of the CAT curve referenced to the NDT point.

these data: the correlations are primarily for steels in the 3/4 to 1-1/4 in. plate thickness range because of test machine limitations, and all tests except the FTE type are for stresses in the order of 1/2 the yield strength. Neither of these limitations is serious, because service failure data for thick sections do not disclose propagation above the CAT curve (as generalized), and explosion bulge tests of 3-in.-thick plate confirm the "plus 60°F" location point for the FTE of thick plates.

It should be noted that *gradient* temperature Robertson tests are not included in this compilation. It has been established by British investigators that the correct CAT is defined by the isothermal temperature test. The Robertson gradient test CAT curve rises sharply at the NDT temperature, somewhat like the vertical line drawn in Fig. 12. This feature has led to the conclusion by British investigators that the NDT correlates with the Robertson gradient test CAT.

These data clearly illustrate that the simple and inexpensive drop-weight test may be used to establish the CAT of a steel, thus eliminating the requirement for conducting time-consuming and expensive series of large-scale crack arrest tests.

EXPERIMENTAL BASIS FOR THE LOCATION OF THE FRACTURE INITIATION CURVES

We shall discuss next the basis for the location in the diagram of the fracture initiation curves for various flaw sizes. It is well-known that with small, sharp cracks loading of the test plate to the yield point is required for fracture initiation at temperatures below the NDT temperature. In effect, this signifies that net section yielding is required for fracture initiation for a small flaw that is not of sufficient length to provide for a significant amount of transfer of stresses from the unsupported central zone to the flaw tip ends. As the flaw size increases, the stress transfer action is accentuated, thus causing yielding to occur at the flaw tip ends for nominal, applied stress levels in the elastic range.

Tests conducted by Battelle Memorial Institute (BMI) investigators Martin and Rieppel for the Ship Structure Committee (7) have contributed important information on the initiation stress for flaws of a wide range of dimensions. These tests involved the use of a 2-ft-diameter "test" section of 3/4-in.-thick steel plate which was insert welded into an alloy steel sphere of 9-ft diameter. The test section steel was a relatively brittle ship plate material with an NDT temperature of 30°F. Flaws of various lengths were introduced into the test section by machining a groove and rewelding, using a brittle weld, as illustrated at the top in Fig. 13. The depth of the brittle cracks ranged from "through" thickness (3/4 in.) to 1/2 thickness (3/8 in.), and the length of these cracks ranged from approximately 4 to 16 in. The sphere was pressurized hydrostatically with chilled brine, resulting in temperatures ranging from 10° to 25°F; thus all tests were conducted below the NDT temperature of the test steel. The sphere was constructed of a quenched and tempered steel having an NDT temperature of approximately −60°F, with the intent of providing for stopping of the crack as it propagated from the test plate into the sphere. Thus, an extensive series of tests was conducted utilizing a single pressure vessel which was weld repaired by the insertion of a new 2-ft-diameter brittle steel section for each flaw size test.

A summary of the fracture initiation stress for the various flaws is provided in Fig. 13 in reference to the fracture analysis diagram of the test steel. The range of fracture stress indicated by the arrow for each flaw size (4, 8, and 16 in.) is caused partly by scatter; however, the fracture stress for the "T" flaws generally reported to the bottom of the range while those of the "1/2 T" flaws reported to the top. The BMI relationships of flaw size and fracture stress are in excellent agreement with failure data, as will be demonstrated in a subsequent section.

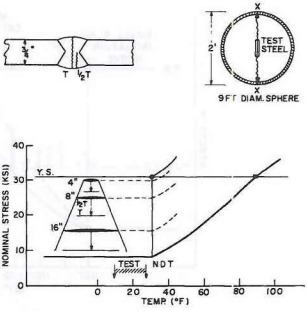

Fig. 13 — Summary of hydrostatic test shell stresses required for the initiation of fracture for flaws of 4, 8, and 16 in. dimensions. All tests were conducted at temperatures ranging from 5° to 20°F below the NDT temperature of the test steel, a 3/4-in.-thick ship plate.

RESIDUAL STRESS RELATIONSHIPS TO THE FRACTURE ANALYSIS DIAGRAM

For the case of structures that do not contain residual stresses, the stress axis of the diagram represents stresses resulting from the applied loads. If residual stresses are present, it is necessary to add the residual stress component to the load stress component. Residual stresses of high order may result in the sum stress exceeding the elastic limit at low levels of applied stresses. In effect, the flaw does not "know" the composite nature of the stress—the fracture event is determined entirely by the "sum" intensity of stress acting on the volume of metal within which the flaw resides. A specific illustration is provided in the top left corner of Fig. 14. This case is concerned with a small flaw located in the weld and HAZ (heat-affected-zone) region which is subjected to a near yield point level of stress resulting from a weld thermal cycle. This type of weld residual stress is known to act in a direction parallel to the weld and to extend for distances of 1 to 2 plate thicknesses from the weld centerline for plates of 1 to 2 in. thickness. For thicker plates the relationship of 1 to 2T does not apply and estimates indicate distances not exceeding 2 to 3 in. In other words, flaws that may be acted upon by such high intensity residual stress fields may be expected to be of short length (small flaws), otherwise the tip of the flaw would extend outside of the peak stress zone. The excellent studies of Wells (8), Hall (9), and others in the area of "low-stress fracture" fit this description. These studies have been based on the use of welded plates featuring small flaws that are cut in the beveled edge prior to welding and remain as "buried" flaws acted upon by high residual weld stresses; in other words, as indicated schematically by the drawing in the top left of Fig. 14.

Now, the fracture analysis diagram interpretation of this situation is that the initiation of a "low-stress" brittle fracture in the testing of such buried flaw test plates is entirely controlled by the fracture initiation curve for small flaws. That is to say, loading to low levels of stress can result in fracture (low-stress fracture by definition) if the temperature is such as to provide for fracture initiation for conditions of incipient yielding at the flaw tip position. This is the case only below the NDT temperature. If appreciable plastic deformation is required to initiate fracture (the case above NDT) the applied stress must necessarily be raised into the plastic range (high-stress fracture by definition). The addition of two components of elastic stress can only produce incipient yielding—gross yielding requires one component to be raised to above the yield point. Obviously, for these tests the only component that may provide for plastic stressing is the applied stress.

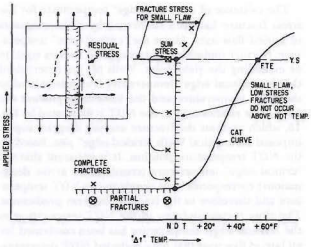

Fig. 14 — Illustrating the fracture analysis diagram prediction that the NDT represents the highest temperature for the initiation of "low-stress" fractures in the presence of high residual stress fields. Complete fractures are predicted for conditions such that the applied stress level exceeds 5 to 8 ksi; short fractures result if the applied stress level is less than this value.

The concept of the controlling effect of the small flaw fracture initiation curve is illustrated in Fig. 14 by the × marks, representing the spectrum of possible fracture stresses for the buried flaw case. Above the NDT temperature the applied stress must be raised to above the yield point as required by the small flaw initiation curve. However, as the temperature is decreased to below the NDT point, fractures may then occur at any applied stress level, depending on the level of the residual stress that is present in the weldment. All that is required is that the sum of the two stresses provide for the development of incipient yielding. The individual lines connecting the × marks with the common point marked "sum stress," Fig. 14, designate the summation of the two stresses for a variety of possible low-stress fracture conditions. If the weld residual stress is very high and therefore fracture initiation occurs at levels of applied stress that are less than the lower shelf for propagation (5 to 8 ksi), the fracture will be arrested on leaving the weld residual stress field; *i.e.*, short fractures will result, as indicated by the circled × marks.

The development of spontaneous fractures in weldments that are not stress relieved is thus indicated to be possible only below the NDT temperature. In such cases, short fractures may develop for conditions such that restraint stresses (long-range "locked in" reaction stresses) outside of the localized field of high residual are less than 5 to 8 ksi. Complete fractures may occur if the restraint stresses are in excess of the 5 to 8 ksi levels.

The existence of a "critical edge" temperature for low stress fracture has been confirmed by all investigators of buried flaw tests. Above the "critical edge" temperature, fracture initiation requires applied stresses equal to or exceeding the yield point. Wells (8) has determined that his "critical edge" temperature is closely related to the NDT temperature and the Robertson *gradient* test CAT. The relationship to the NDT is illustrated by Fig. 15, which presents the fracture analysis diagram superimposed on a typical Wells "critical edge" plot, based on the NDT temperature position. It is apparent that the "critical edge" temperature (crosshatched arrow designations) corresponds very closely to the NDT temperature and therefore to the fracture diagram predictions. The close correspondence of the NDT temperature to the "critical edge" temperature has been confirmed for all buried flaw tests that have included NDT determinations for the test steels.

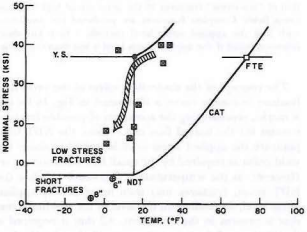

Fig. 15 — Wells (8) data points which define the critical edge temperature for low-stress fracture superimposed on the fracture analysis diagram of the test steel: 1-in. plate, 0.14% C, 1.07% Mn, 0.02% Si.

Figure 16 illustrates a replot of Hall, Nordell, and Munse's (9) data superimposed on the fracture analysis diagram. Most of these tests were concentrated at −40°F for purposes of a positive demonstration of the influences of notch preparation methods and techniques for eliminating low-stress fractures. Comparison of the results obtained at 15° to 40°F with a single test at 0°F clearly illustrates the critical edge effect. Hall, Nordell, and Munse also found that "hot loading" at 100°F (NDT + 90°F) mechanically stress relieved the buried flaw, resulting in the elimination of "low-stress fracture". Similar results were obtained with stress relief at 1150°F, as was also noted by Wells. It may be concluded that in the absence of a weld residual stress

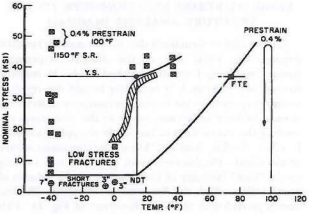

Fig. 16 — Hall, Nordell, and Munse (9) data points which define the critical edge temperature for low-stress fracture superimposed on the fracture analysis diagram for the test steel: 1-in. plate, ASTM A212-B, 0.30% C, 0.75% Mn, 0.26% Si.

the applied stress must exceed yielding for the case of a small flaw, as indicated by the small-flaw fracture initiation curve of the fracture analysis diagram.

As will be evident from the presentation of service failure data, all failures of welded structures which could be ascribed to small flaws in the presence of weld residual stresses (structure not stress relieved) occurred at temperatures below the NDT of the steel, confirming the "critical edge" effect and the fracture diagram predictions.

The foregoing discussions were concerned with small-flaw fracture initiation from locations of intense but localized residual stress fields. We shall now discuss the fracture analysis diagram predictions for the case of fracture initiation due to large flaws under the influence of restraint stress fields. The differentiation between "residual" and "restraint" stresses is simply one of extent and source. By restraint stresses we mean the "locked in stresses" outside of the immediate boundaries of the weld zone region. Such long range stresses are generally considered not to exceed approximately 1/2 the yield strength of the metal. Figure 17 illustrates a possible situation featuring a long weld crack that is loaded by a restraint stress field of approximately 1/2 the yield strength intensity. We may assume that the flaw is sufficiently large (say 1 to 2 ft) so as to cause a close approach of the fracture initiation curve to the CAT curve for the specified stress level. In effect, we are stating a case such that a practical approach involves using CAT curve protection to establish fracture safety. This is obtained by limiting the service to temperatures in excess of NDT + 30°F, as indicated by the illustration.

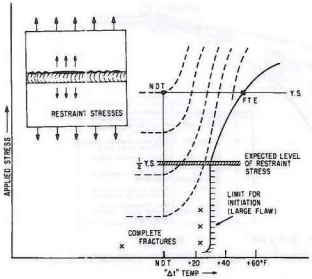

Fig. 17 – Illustrating the fracture analysis diagram prediction that large flaws located in restraint stress fields (of 1/2 the yield strength) may result in low-stress fracture initiation at temperatures below the CAT (NDT + 30°F)

The × points indicate that low-stress fracture at temperatures less than NDT + 30°F are possible. Complete fractures may result at low levels of applied stress because the extensive stress field required for propagation over long distances is provided by the restraint stress.

The above case may be recognized as the basic premise for design based on CAT data. The proponents of this approach make a basic *assumption* that large flaws may be anticipated in the structure and therefore fracture initiation is possible at all temperatures below the CAT for the general level of stress in the structure. On a fracture analysis diagram basis the requirement for restricting service to temperatures in excess of NDT + 30°F follows only if the anticipated flaw length is in excess of 1 ft. Accordingly, a basis is provided for the application of engineering judgment based on flaw size expectancy analyses. Such a basis is not provided by the invariant use of CAT principles. If CAT principles were applied to the case of ship steels, the documented sufficient improvement of ship steel quality by a 30°F reduction of NDT temperatures would have been deemed inadequate for the solution of the World War II ship fracture problem. In effect, a 60°F improvement would have been indicated – such an improvement would have required the change to a much more expensive, normalized ship steel. The significance of these statements will become more apparent in the section on ship fracture steels, illustrated in Figs. 40 and 41.

VALIDATION OF THE FRACTURE ANALYSIS DIAGRAM – SERVICE FAILURES AND PRESSURE VESSEL TESTS

A long term interest of the authors in failure analysis, involving both service failures and simulated service tests, resulted in the accumulation of a large body of data which now provides for critical evaluation of the validity of the fracture analysis diagram concepts. We shall now present all of the service failure data that are available as of the date of the preparation of this report – none have been omitted. Results of pressure vessel tests will be presented also; these tests involved the pressurization of deliberately flawed vessels and provide data of direct significance to the service performance of pressure vessels.

The first step in conducting service failure analyses is the determination of the location of the fracture analysis diagram on the temperature scale. This step simply requires the determination of the NDT temperature of the fracture source material (near the fracture origin) by means of the drop-weight test or indirectly by means of the Charpy V test. If the Charpy V test is used it is necessary to have prior information of the Charpy V energy-NDT correlation for the type of steel involved. For the purposes of this report we shall refer, with one exception, to NDT temperatures established directly by the use of the drop-weight test.

The second step involves the placing of a suitable notation at the temperature of the service failure. A vertical line drawn in the fracture diagram at the service temperature position serves this purpose.

The third step involves the determination of stress levels relative to the initiation and propagation of the fracture. The initiation stress may include both applied and residual stresses.

The fourth requirement involves the determination of the flaw size. This ordinarily requires visual examination.

In effect, the described steps constitute a straightforward process of placing the fracture analysis diagram at the proper position in the temperature scale, locating a stress-temperature "point" in the diagram, and assigning a flaw size to this point. The required information is usually readily available within the limits required for the simple interpretation of the fracture analysis diagram. In fact, the simplicity of the analysis operation is one of the principal virtues of the proposed plan.

The service failure and pressure vessel test cases to be described have been separated into various categories which correspond to specific zones of the fracture

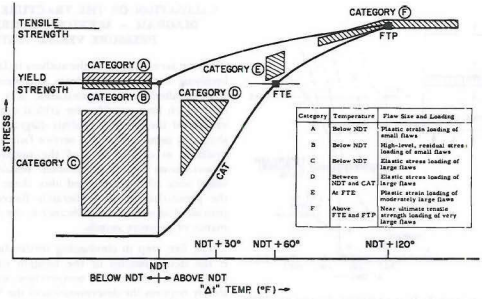

Category	Temperature	Flaw Size and Loading
A	Below NDT	Plastic strain loading of small flaws
B	Below NDT	High-level, residual stress loading of small flaws
C	Below NDT	Elastic stress loading of large flaws
D	Between NDT and CAT	Elastic stress loading of large flaws
E	At FTE	Plastic strain loading of moderately large flaws
F	Above FTE and FTP	Near ultimate tensile strength loading of very large flaws

Fig. 18 — Sequence of the discussion of failure-analysis cases is indicated by categories A to F referenced to various zones of the fracture analysis diagram

analysis diagram. Figure 18 illustrates the location of these zones; the corresponding categories are defined as tabulated in the figure. In effect, the course of the presentation will provide a step by step validation of the various zones of the fracture analysis diagram.

Category A: Temperature Below NDT — Plastic Strain Loading of Small Flaws

Case A1: Heavy Section Pressure Vessel Forging, ASTM A293 Steel

Composition (Wt—%)								
C	Mn	Si	P	S	Ni	Cr	Mo	V
0.28	0.64	0.15	0.010	0.013	2.56	0.23	0.52	0.06

Y.S. (ksi)	T.S. (ksi)	El. (%)	R.A. (%)
96.0	116.0	18.0	48.0

NDT (°F)	C_vNDT* (ft-lb)	FT (°F)	C_vFT* (ft-lb)
130	30	70	18

*Designation to be used hereafter for average Charpy V energy values at NDT temperature (C_vNDT) and at failure temperature (C_vFT).

Figure 19 illustrates the fracture of a 100-ton pressure vessel of 9-1/2-in. wall thickness at the region of primary fracture. The vessel was subjected to slow, cyclic, hydraulic pressurization to 30 ksi shell stress at a constant operating temperature of 70°F. A threaded closure provided access to the interior. After 1550 cycles, representing several months of operation for the new vessel, a small fatigue crack of 1/8-in. depth developed at the root of the first thread, which was subjected to a small amount of reversed (tension-compression) plastic deformation on each cycle. The brittle fracture which initiated from this small flaw resulted in splitting off a 20-ton section which represented the bottom head of the pressure vessel. The "flat break" appearance of the fracture through the 9-1/2-in. wall and the fatigue crack at the root of the thread are illustrated in Fig. 20. The vessel was constructed as a one-piece cylindrical forging of ASTM-A293 composition, which represents a typical Ni-Cr-Mo-V steel for heavy forgings. The NDT temperature of the steel was 130°F.

The fracture analysis diagram (Fig. 21) illustrates that the failure of the vessel was in conformance to predictions for conditions of a small flaw, over yield stress loading at the position of the flaw, and service temperature below the NDT. It is noted that a secondary fracture propagated longitudinally through the shell at a stress level of 30 ksi and stopped on reaching the closure region of the top head, at which point the shell stress was below 8 to 10 ksi.

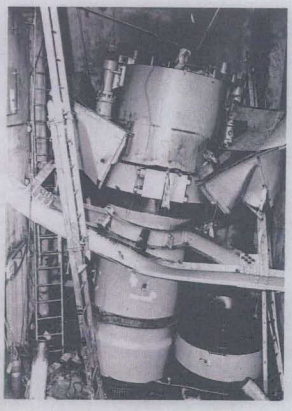

Fig. 19 – (Case A1) Fracture of a 100-ton pressure vessel; the bottom head, shown at right, swung out bottom-side up prior to the fall of the vessel. The ladders indicate the size.

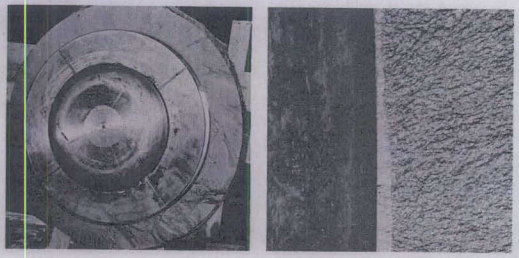

Fig. 20 – (Case A1) Brittle fracture face of the 9-1/2-in. shell wall of the 100-ton pressure vessel. The enlargement shows the 1/8-in.-deep fatigue crack (shiny region) located at the root of the thread.

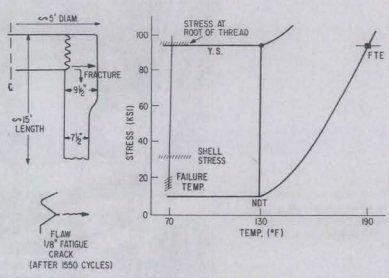

Fig. 21 – (Case A1) Fracture analysis relating to the service failure of the 100-ton, forged, ASTM A293 pressure vessel

Case A2: Anchor Windlass – Shaft Coupling, SAE 1050 Forged Steel

Composition (Wt–%)						
C	Mn	Si	P	S	Ni	Cu
0.53	0.79	0.26	0.024	0.030	0.23	0.21

Y.S. (ksi)	T.S. (ksi)	El. (%)	R.A. (%)
42.3	89.7	22.5	42.0

NDT (°F)	C_vNDT (ft-lb)	FT (°F)	C_vFT (ft-lb)
100	8	70	5

Figure 22 illustrates the fracture of an anchor windlass-shaft coupling on a Coast Guard vessel. The fracture developed through both sides, following the corners of sharp, 1/16-in.-fillet keyways. The broken halves were projected outward for a considerable distance, indicating that the anchor was housed under power and therefore resulted in severe overload conditions at the keyways. The coupling represented an SAE 1050 forging.

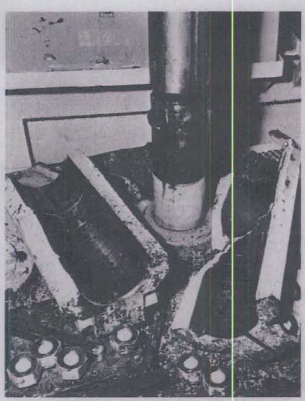

Fig. 22 – (Case A2) Fracture of an anchor windlass-shaft coupling

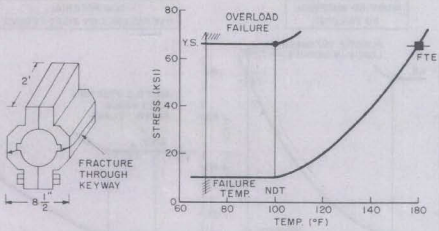

Fig. 23 – (Case A2) Fracture analysis relating to the overload failure of the forged, SAE 1050, anchor windlass-shaft coupling

The failure temperature is indicated on the fracture analysis diagram (Fig. 23) to have been 30°F below the NDT temperature of the steel. The plastic overload developed at the keyway fillet is indicated by plotting the initiation stress at slightly above the yield strength of the steel. The only flaws present at the keyway consisted of machine marks.

Cases A3 to A7: Heavy Section Cast Propellers, AISI Type 410 Stainless Steel

Composition Range (Wt – %)					
C	Mn	Si	P	S	Cr
0.08/0.12	0.66/1.02	0.80/1.19	~0.02	~0.03	11.7/12.6

Y.S. (ksi)	T.S. (ksi)	El. (%)	R.A. (%)
37.0/45.0	55.0/75.0	5.0/17.0	5.0/21.0

NDT (°F)	C_vNDT (ft-lb)	FT (°F)	C_vFT (ft-lb)
*	*	30/40	5/7

*For each case, the NDT was 200°F or higher (no tests, drop-weight or Charpy, were conducted at higher temperatures).

Figure 24 illustrates a typical fracture of a cast, 12% Cr, AISI Type 410 stainless steel propeller previously used for icebreaker service. Five failures occurred in rapid sequence on initial use of the new type of propeller during the early 1950's. Icebreaker service requires that the propellers endure plastic deformation overloads, which obviously was not within the capability of this material in the presence of numerous small casting defects and deep chipping hammer marks. Broken stub ends were investigated by the authors and found to involve material based on a poor choice of chemical composition and heat treatment practice. The fracture analysis diagram of Fig. 25 (right) summarizes the results for the Cases A3 to A7 failures. The inadequacy of the material for plastic overload service at ice-water temperature, in the presence of small defects is in conformance with predictions of the fracture diagram.

A solution to the icebreaker propeller problem was found by developing a modified type 410 stainless steel,

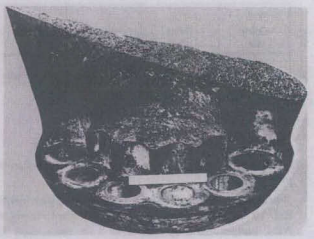

Fig. 24 – (Cases A3 to A7) Typical fracture of cast 12% chromium stainless steel propellers previously used for icebreaker service. Dimensions are indicated by the 12-in. rule.

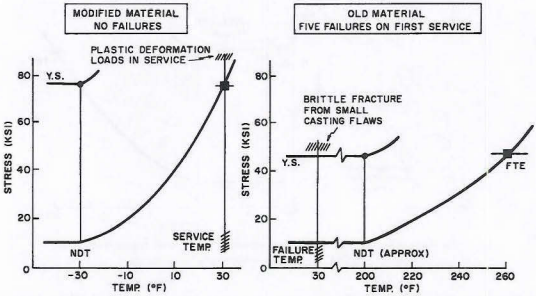

Fig. 25 – (Cases A3 to A7) Fracture analysis relating to the overload failures of cast 12% chromium stainless steel propellers (right); note that the service temperature was below the NDT temperature. Improvement in the steels resulted in shifting the NDT temperature to 60°F below the service temperature. For the improved propeller steels, the fracture analysis diagram (left) predictions for safe performance under overload conditions were justified.

featuring low silicon and additions of molybdenum and nickel, as follows:

Nominal Composition (Wt–%)					
C	Mn	Si (Max)	Mo (Min)	Ni	Cr
0.12	0.80	0.50	0.50	0.75	12.0

Y.S. (Min) (ksi)	T.S. (Min) (ksi)	El. (Min) (%)	R.A. (Min) (%)
65.0	90.0	18.0	30.0

NDT (°F)	C_vNDT (ft-lb)
<–30	20

Optimum heat treatment of this material resulted in improved strength properties and ductility.

A complete report of this investigation is provided by Ref. 10. The primary aim of the study was to lower the NDT temperature, of cast, 4 to 5 in. thick, type 410 material to below –30°F. In effect, this improvement guaranteed that the FTE temperature (NDT + 60°F) would be no higher than the ice-water (30°F) service temperature of the propellers. The improvement that was obtained is indicated by the fracture diagram of Fig. 25 (left). The modified propellers have since endured severe plastic overload service, including being deformed out of useful shape, without failure. The fracture diagram predicts that at the service temperature, extremely large (and unlikely) flaws on the order of 1 ft or more would be required to initiate failure of the new propellers under expected conditions of plastic overload.

Case A8: Pressure Vessel, ASTM A302–Grade B Steel

Composition (Wt.–%)						
C	Mn	Si	P	S	Cr	Mo
0.19	1.24	0.29	0.024	0.029	0.23	0.51

Y.S. (ksi)	T.S. (ksi)	El. (%)	R.A. (%)
36.1	68.0	52.3	46.8

NDT (°F)	C_vNDT (ft-lb)	FT (°F)	C_vFT (ft-lb)
70	10	60	9

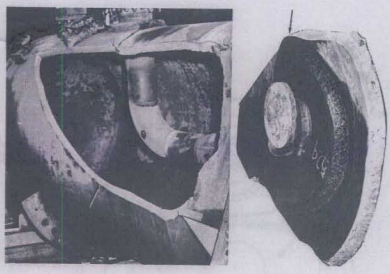

Fig. 26 – (Case A8) Hydrostatic test fracture of a 7.5-ft-diameter, 3-in.-thick, stress relieved, ASTM A302-B pressure vessel. The fracture origin is indicated by the arrows.

This case involves a 3-in.-thick, stress relieved, A302B pressure vessel that failed in hydrostatic test, as illustrated by Fig. 26. The initiating flaw involved a 1-1/2 × 3/4 in. weld crack, located at the toe of a fillet weld of a manhole reinforcement pad on the inside of the shell plate. Details of the crack location and fracture path are illustrated in Fig. 27. The low level of yield strength of this material, which normally should develop a yield strength in the range of 60 to 65 ksi, resulted in the disclosure that the plate had inadvertently been annealed (furnace cooled from 1650°F) in place of the required normalizing heat treatment (air cool from 1650°F). Following fabrication the vessel was stress relieved at 1150°F.

The full hydrostatic test stress was applied to the vessel at the time of failure. The level of the shell stress, 38 ksi, closely matched the yield strength of the annealed vessel, as indicated in the fracture diagram of Fig. 27. The failure temperature was approximately 15°F below the NDT temperature of the shell plate.

It is interesting to note that, in the absence of a tensile test, to reveal that the actual yield strength was 1/2 that expected, this particular failure would be deemed not to conform to the fracture diagram prediction: *i.e.*, the flaw is too small to provide for fracture initiation at stress levels of 1/2 the expected yield strength of the steel, considering that the residual stresses are low due to stress relieving of the vessel. The fact that the yield strength of the shell plate was essentially 1/2 of the expected value completely explains the failure in terms of the fracture diagram and places it in the plastic strain loading of small flaw category of service failures.

Category B: Temperature Below NDT – High-Level, Residual Stress Loading of Small Flaws

Case B1: Spontaneous Pressure Vessel Fracture, ASTM A302, Grade B Steel

Composition (Wt – %)					
C	Mn	Si	P	S	Mo
0.20	1.19	0.18	0.021	0.031	0.56

Y.S. (ksi)	T.S. (ksi)	El. (%)	R.A. (%)
63.3	85.4	24.2	51.4

NDT (°F)	C_vNDT (ft-lb)	FT (°F)	C_vFT (ft-lb)
100	32	60	20

During the period of investigation of Case A8, a companion 2-9/16-in. thick, A302B pressure vessel of similar design to that shown in Fig. 26, developed a spontaneous brittle fracture. The fracture occurred with a loud report, during an off-work night, while the vessel was partly fabricated. The initiation point of the failure was traced to small heat affected zone cracks at the toe of a fillet weld for a manhole port reinforcement plate, as illustrated by Fig. 28, left. The fracture progressed in both directions for a distance of 8 ft and then stopped. The origin and propagation paths of the crack were

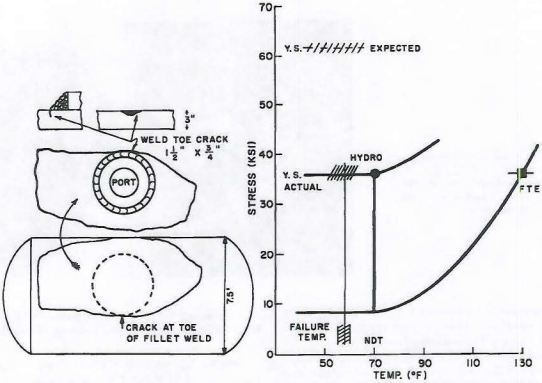

Fig. 27 – (Case A8) Fracture analysis relating to the hydrotest failure of the stress relieved ASTM A302-B pressure vessel. The steel was given an annealing heat treatment by error which resulted in hydrotest shell stresses equal to the yield strength level.

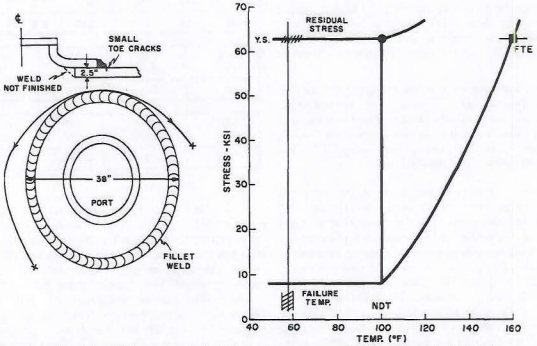

Fig. 28 – (Case B1) Fracture analysis relating to the spontaneous fracture of a partially fabricated ASTM A302-B pressure vessel

obviously related to a residual stress system of the port-plate fillet weld.

The failure temperature of the steel was approximately 40°F below the NDT temperature. The fracture analysis diagram (Fig. 28) illustrates the conditions of yield-point-level weld residual stress which combined with the presence of small HAZ (heat-affected-zone) cracks to cause spontaneous fracture of the vessel.

Case B2: Weld Repaired Pressure Vessel, ASTM A212 Grade B (Equivalent) Steel

Composition (Wt – %)				
C	Mn	Si	P	S
0.33	0.62	0.24	0.029	0.039

Y.S. (ksi)	T.S. (ksi)	El. (%)	R.A. (%)
37.9	77.4	25.5	

NDT (°F)	C_vNDT (ft-lb)	FT (°F)	C_vFT (ft-lb)
80	8	60/70	6

This case involved a 1-1/4-in.-thick, 5-ft-diameter pressure vessel that had been used in chemical processing for approximately 20 years. Because of localized thinning of the wall due to corrosion, it was repaired by the use of patch plates which were welded to the interior shell surface. Four plates of 16-in.-width (manhole port size) were used. In effect, the patch plates were held in place by fillet welding of the four sides of the composite. The shell served as the "backup plate" for the two butt welds of the patch plate assembly. The vessel was repaired "in place" and was not stress relieved. Small weld cracks that extended into the "backup" position of the central welds provided the flaws for the initiation of fracture of the shell on a routine hydrotest (Fig. 29). Details of the shell fracture, the location of the patch plates, and the point of fracture origin at the longitudinal through weld are illustrated in Fig. 30, left.

The chemical analysis and mechanical properties were found to be equivalent to those currently specified for ASTM A212 Grade B. The failure temperature was approximately 15°F below the NDT temperature of the shell plate. The fracture analysis diagram (Fig. 30) illustrates a typical failure case for weldments that have not been stress relieved – small weld cracks, high residual stress, and failure temperature below the NDT temperature. Fracture propagation was assured by the general level of hydrostatic shell stress of approximately 20 ksi.

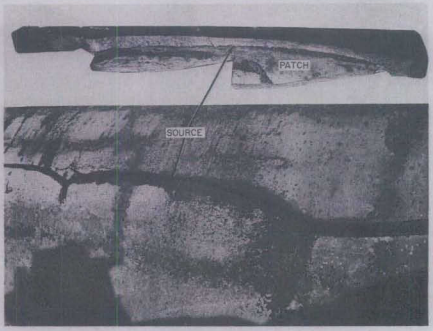

Fig. 29 – (Case B2) Hydrotest fracture of a 20-year-old pressure vessel following patch plate salvaging repair of the inside surface; the fracture origin is shown above.

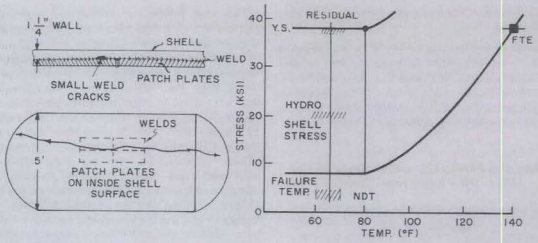

Fig. 30 — (Case B2) Fracture analysis relating to hydrotest failure of the patch-plate-repaired ASTM-A212-B pressure vessel. The vessel was not stress relieved after completion of the weld repairs.

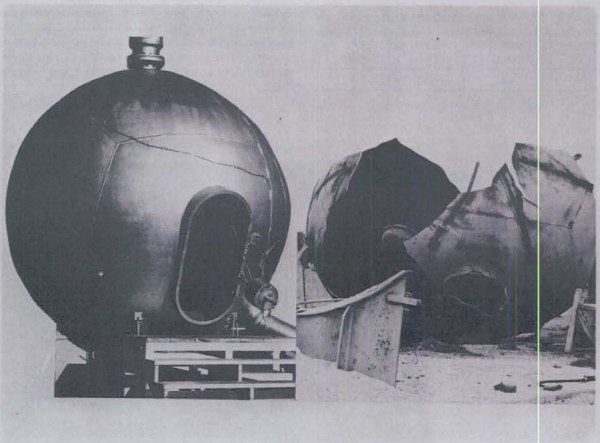

Fig. 31 — (Case B3) Blast chamber prior to fracture (left) and after fracture (right)

Case B3: Blast Chamber Pressure Vessel, ASTM A285 Grade C Steel

Composition (Wt–%)					
C	Mn	Si	P	S	Cu
0.25	0.45	0.01	0.007	0.024	0.28

Y.S. (ksi)	T.S. (ksi)	El. (%)	R.A. (%)
61.3	70.5	23.0	58.0

NDT (°F)	C_vNDT (ft-lb)	FT (°F)	C_vFT (ft-lb)
90	6	60	5

The blast chamber shown in Fig. 31, left, was used for muffling the sound resulting from the testing of small amounts of experimental explosives. These chambers are widely used by the explosives industry. The fractured remains of the chamber (Fig. 31, right) resulted from a standard test explosion which developed a shell stress not exceeding 15 ksi. As illustrated in Fig. 32, left, the fracture initiated from a small weld crack located at the intersection of the shell with the door port. The crack was located in the shell plate side of the weld on the inside surface and was identified readily by chevron marks pointing to a rusted area approximately 1 in. long and 3/8-in. deep. The pressure vessel was not stress relieved. The 3/4-in. shell plate was purchased to ASTM A285C.

The fracture analysis diagram (Fig. 32, right) illustrates that the failure temperature was 30°F below the NDT. The combination of a small weld crack and high weld residual stresses provided the necessary conditions for initiation of the fracture. The fracture surfaces showed very thin shear lips typical of fractures below the NDT temperature.

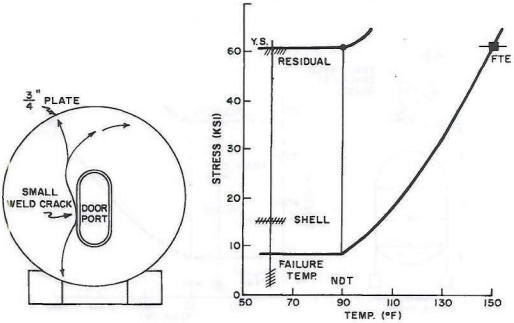

Fig. 32 – (Case B3) Fracture analysis relating to service failure of the ASTM A285-C blast chamber. The vessel was not stress relieved.

Case B4: Large Storage Tank Pressure Vessel, ASTM A285 Grade C Steel

Composition (Wt – %)					
C	Mn	Si	P	S	Cu
0.20	0.37	0.05	0.005	0.025	0.06

Y.S. (ksi)	T.S. (ksi)	El. (%)	R.A. (%)
38.1	61.2	30.5	58.3

NDT (°F)	C_vNDT (ft-lb)	FT (°F)	C_vFT (ft-lb)
60	6	45	5

This case represents a hydrostatic test failure of a large, 70-ft-high by 45-ft-diameter, pressure vessel for petroleum refinery operations. Figure 33, left, illustrates that the fracture initiated in the 1-1/4-in. knuckle plate of the bottom head, at the toe of a weld which connected the knuckle plate to a supporting 7/8-in. skirt plate. The fracture propagated through the bottom head and lower regions of the vessel, resulting in fragmentation of this region into 25 or more pieces. The efflux of the water from the shattered bottom resulted in the development of a vacuum in the top region of the vessel with consequent crumpling, as if it had been squeezed by a giant press (Fig. 34).

The chevrons pointed to the indicated source point; however, local damage to the fracture at this point prevented positive identification of crack defects. It was concluded that such defects as existed were obviously of small dimensions and probably represented small weld cracks at the toe of the weld.

The fracture analysis diagram (Fig. 33, right) illustrates that the failure temperature was 10° to 15°F below the NDT temperature. The level of hydrostatic shell stress for the cylindrical portion of the shell was 18 ksi. At the knuckle position the stress is estimated to be in the order of 25 ksi. In the absence of flaws of sufficient size to trigger at this level of stress, it is concluded that the fracture originated from the combination of small crack defects and high weld residual stresses.

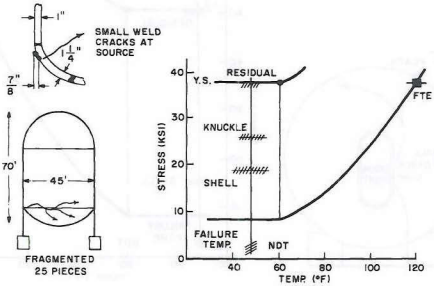

Fig. 33 – (Case B4) Fracture analysis relating to hydrotest failure of a 45-ft-diameter ASTM A285-C storage tank. The vessel was not stress relieved.

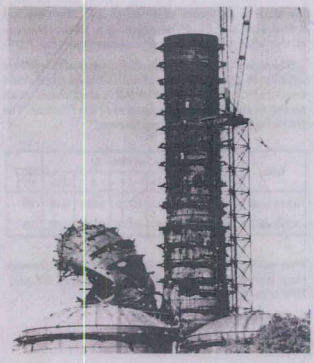

Fig. 34 — (Case B4) Hydrotest failure of the 45-ft-diameter, ASTM A285-C storage tank. The top region of the vessel was crumpled because of the vacuum which developed within by the efflux of water from the shattered bottom head (not visible).

Case B5: CO Converter Pressure Vessel, ASTM A204 Grade B Steel

Composition (Wt – %)					
C	Mn	Si	P	S	Mo
0.19	0.78	0.24	0.010	0.012	0.64

Y.S. (ksi)	T.S. (ksi)	El. (%)	R.A. (%)
52.4	77.5	25.0	

NDT (°F)	C_vNDT (ft-lb)	FT (°F)	C_vFT (ft-lb)
110	7	45	4

The hydrostatic failure of a 30-ton, 26-ft-long, 7.5-ft-diameter pressure vessel fabricated for use as a CO converter is shown in Fig. 35. The arrow points to the region of fracture initiation at the toe of a reinforcing pad weld. Design details at the point of initiation are given in Fig. 36, left.

In compliance with code requirements, the top third of the vessel was constructed with A204 steel (900°F operation) and the bottom two-thirds of the vessel were constructed with A212 steel (850°F operation). For

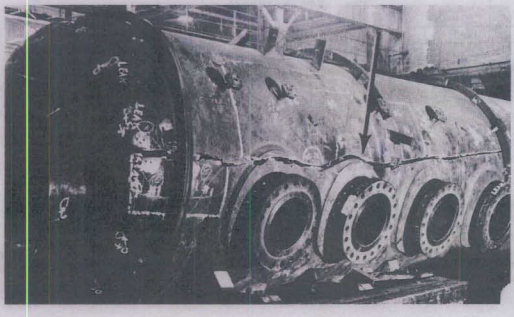

Fig. 35 — (Case B5) Fracture of a 7.5-ft-diameter CO converter pressure vessel. The arrow points to the fracture source region.

corrosion resistance purposes, type 304 stainless steel liner sheet was plug welded to the inner surface of the vessel. To avoid corrosion sensitization of the liner, the vessel was stress relieved at the relatively low temperature of 950°F for 10 hours.

The source of the fracture was located in the A204 shell region. The fracture traversed the full length of the A204 and A212 shell sections and continued through the A204 head which joined to the A204 shell section. The shell stress was approximately 25 ksi.

The fracture analysis diagram (Fig. 36, right) illustrates that the failure temperature was approximately 60°F below the NDT temperature of the A204 source plate. The decrease in weld residual stress resulting from a 950°F stress relief treatment is expected to be relatively minor, particularly for this grade of steel. Considerations of the geometric features of the port opening and the minor stress relief resulting from the stated treatment, suggest a stress state at the position of the flaw in the order of 40 to 45 ksi. The observed 3 × 0.4-in. flaw would be expected to initiate fracture at this level of stress at temperatures below the NDT.

There are two other interesting aspects of this failure relating to the properties of the 1-3/4-in.-thick A204 head and the 1-13/16-in.-thick A212 shell plates which served to continue the propagation of the fracture. The following data are of primary interest:

Item	Composition (Wt – %)						NDT (°F)
	C	Mn	Si	P	S	Mo	
A204 head	0.19	0.90	0.27	0.010	0.023	0.52	80
A212 shell	0.27	0.76	0.20	0.013	0.023	0.02	70

The propagation of the fracture at 45°F, through plate material having NDT temperatures of 80° and 70°F is to be expected.

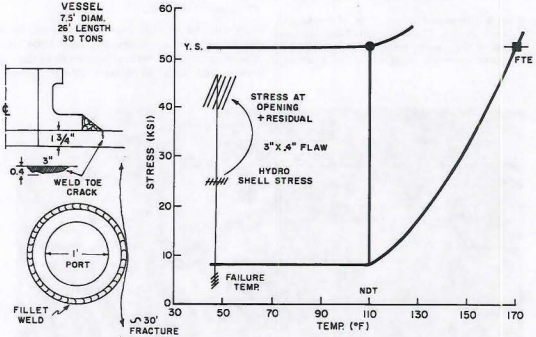

Fig. 36 – (Case B5) Fracture analysis relating to the hydrostatic test failure of the CO converter pressure vessel. The data relate to the ASTM A204 portion, which was the initiation point. The vessel was given an inadequate stress relief at 950°F.

Case B6: World War II Ship Steel

Composition (Wt. – %)				
C	Mn	Si	P	S
0.25	0.45	0.04	0.010	0.028

Y.S. (ksi)	T.S. (ksi)	El. (%)	R.A. (%)
29.6	61.9	40.3	61.1

NDT (°F)	C_1 NDT (ft-lb)	FT (°F)	C_1 FT (ft-lb)
50	10	35	8

In 1947 the T-2 tanker USS Ponaganset fractured into two sections while tied at dockside in Boston, Mass. Figure 37 illustrates the general appearance of the vessel; details of the fracture origin are presented in Fig. 38, left. The source of the fracture was an arc strike located at the toe of a fillet weld that joined a chock to the deck. Figure 39 illustrates the fine network of sharp cracks that are generally associated with arc strikes. The presence of the sharp cracks in the arc strike located in a region of high residual stress resulting from the fillet weld provided the necessary conditions for fracture initiation at temperatures below the NDT. As indicated by the fracture analysis diagram, the failure temperature was 15°F below the NDT temperature of the source plate. The steel was typical of the World War II production material which features relatively high carbon and low manganese contents.

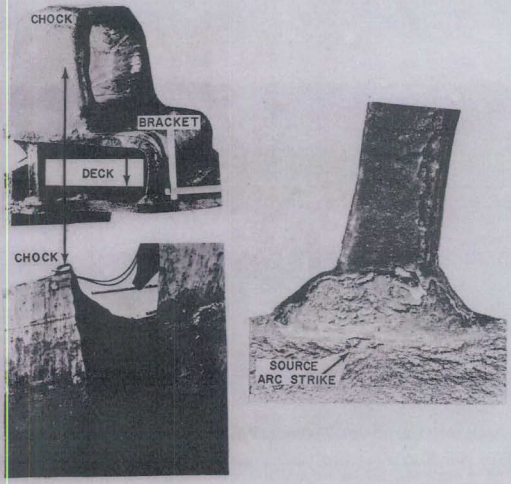

Fig. 37 – (Case B6) Fracture of the T-2 tanker Ponaganset. The fracture origin was traced to an arc strike, located in the deck plate as indicated (bottom right).

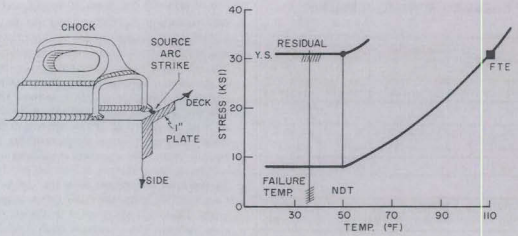

Fig. 38 – (Case B6) Fracture analysis relating to the dockside failure of the T-2 tanker Ponaganset

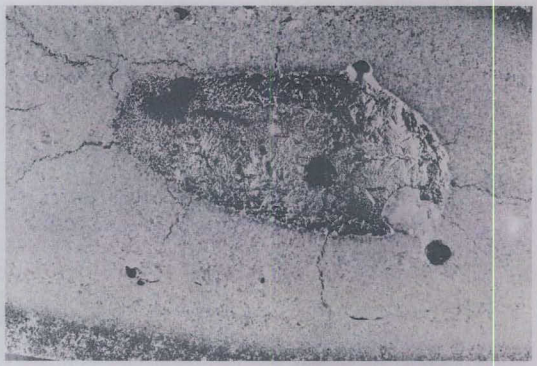

Fig. 39 – Network of 1/8 to 1/4-in. cracks generally associated with arc strikes. The crater dimensions are approximately 1/4 in. by 1/8 in. The small size of the flaws that are sufficient to trigger failure in the presence of high residual stress fields at temperatures below the NDT temperature is emphasized by this illustration.

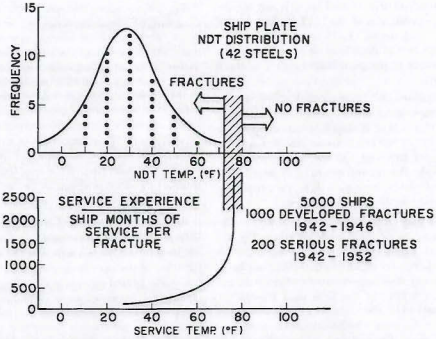

Fig. 40 — Illustrating that no failures of World War II ships occurred at temperatures above the 70°F upper limit of the NDT frequency distribution range of World War II ship steels. A high rate of fracture per month of service occurred at temperatures of 30° to 50°F, for which 20 to 50% of the steels were below their NDT temperatures.

Figure 40 illustrates the service experience record of World War II ships, correlated to the NDT frequency distribution of the steels used for ship fabrication. The mean NDT temperature is noted to be approximately 30°F; the highest and lowest NDT temperatures are indicated by the ends of the frequency curve to be in the order of 70° and 0°F, respectively. The NDT frequency plot is in exact correlation with the ship service experience, as follows:

1. No fractures occurred at service temperatures above the 70°F upper limit of the NDT frequency distribution curve.

2. The ship months of service per fracture decreased rapidly with decreasing temperature in the range 70° *to* 30°F. This range is marked by the increase in the number of steels of below NDT temperature characteristics from 0% at 70°F to approximately 50% of the statistical population at 30°F.

If another frequency distribution curve is drawn representing the CAT for stresses in the order of 1/3 to 1/2 the yield strength of the World War II ship plates, an explanation of the complete fracture of the Ponaganset is obtained. The CAT distribution curve (Fig. 41) is represented by temperatures 30°F higher than noted for

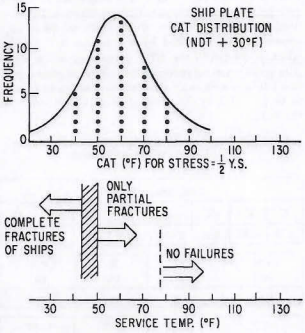

Fig. 41 — Illustrating that complete failure of ships occurred only at temperatures such that essentially *all* of the ship steels were below their respective CAT

the NDT frequency distribution. This is based on the fracture diagram prediction of the CAT at the levels of general stress of ship decks, *i.e.*, 12 to 15 ksi. Actually, the stress of ships tied at dock may be on the high side of the range because of the poor ballasting represented by an empty ship.

The CAT frequency distribution curve indicates that, at the failure temperature of 35°F, essentially *all* of the steels used for World War II ship fabrication would be expected to be below the crack arrest temperature for the service stresses involved. As the result, the complete fracture of the Ponaganset was to be expected inasmuch as no steel plates having crack arrest properties were to be expected in the line of fracture.

A general case may be made from ship failure statistics, as indicated by the diagram at the bottom of Fig. 41. All failures which occurred at temperatures of 50° to 70°F involved the fracture of a limited number of plates. The CAT frequency distribution curve indicates that at 60°F approximately 50% of the ship steel population would be expected to be above the CAT, *i.e.*, would act as crack arresters. Failures which occurred at temperatures below 45°F often involved the total, or almost total, fracture (Class I fractures) of the ship. The case of the Ponaganset thus fits the general experience.

The NDT frequency distribution curve and the NDT derived CAT distribution curve provide a *remarkably* exact prediction of World War II ship fracture experience in terms of the fracture analysis diagram. Irrespective of welding variables, the failures of these ships appear to be controlled by a common denominator which is related to the NDT properties of the steels. The initiation stress required for failures resulting from small defects such as arc strikes and weld cracks appears to be provided by the residual stresses associated with the welds.

Case B7: Retaining Ring for Aluminum-Extrusion Container, ASTM A293 Steel

Composition (Wt–%)							
C	Mn	Si	P	S	Cr	Mo	V
0.30	0.85	0.22	0.010	0.010	0.78	1.18	0.20

Y.S. (ksi)	T.S. (ksi)	El. (%)	R.A. (%)
142.1	157.2	11.5	28.5

NDT (°F)	C_vNDT (ft-lb)	FT (°F)	C_vFT (ft-lb)
400	15	70	5

This case involves the spontaneous fracture of a large ring forging, resulting from the presence of very small cracks and high local residual stresses. Figure 42 illustrates the large size of the subject forging, which served as one of five retaining rings for an extrusion press container assembly. The function of the retaining rings is to provide prestress (shrink fit) containment for the inner, hot work alloy liner of the extrusion chamber which normally operates at temperatures on the order of 700° to 900°F for purposes of extruding aluminum. This press was the largest ever built for extruding aluminum; at the time of the ring fracture the new press was in the process of checkout preliminary to production use.

Because of problems of high temperature operation (11), it became necessary to determine the temperatures attained in the outer surface of the retaining rings as a function of the operating temperature conditions of the internally heated extrusion chamber liner. For this purpose, thermocouples were silver brazed to the face of one of the rings by means of an oxyacetylene torch. The brazing was performed while the container assembly was at room temperature. After brazing the assembly remained overnight at room temperature. Next morning, prior to use of the assembly, a brittle fracture (loud noise) developed across the 12 × 13-in. section of the

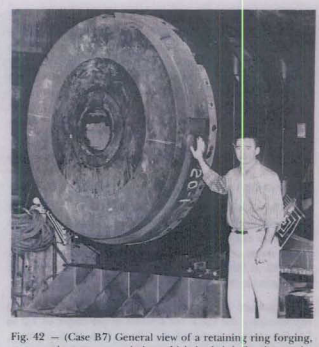

Fig. 42 — (Case B7) General view of a retaining ring forging, representing an external ring which is shrink fitted over the (dark) core of an extrusion chamber section. The chamber assembly comprises five adjoining rings.

ring, as shown in Fig. 43. The source of the fracture was traced to a cluster of microcracks developed in the area of silver brazing.

Fig. 43 – (Case B7) Fracture face (12×13-in.) of the extrusion chamber retaining ring. Fracture source markings are at one of the positions of thermocouple attachment by brazing; note a companion thermocouple.

The stress conditions which caused the initiation and propagation of the fracture are indicated in Fig. 44. The microcracks were located in the region of yield point level residual stress resulting from the localized torch heating to red heat. The combination of small cracks and high residual stresses provided for the initiation of the fracture. Propagation of the fracture across the section was then assured by the presence of shrink fit stresses in the order of 50 ksi.

The ring forging conformed to ASTM A293-55T Class 8 steel, which represents a Cr-Mo-V forging grade that has been used extensively for extrusion press and other service involving temperatures in the range 700° to 900°F. The subject composition was developed primarily for creep resistance properties. Because of the low tempering temperature used to develop high creep resistance, the NDT temperature of the steel was very high (400°F). Thus, the failure temperature (70°F) was far below the NDT temperature. However, as illustrated by the fracture analysis diagram (Fig. 44, right) the same considerations apply as for the case of failures which developed at temperatures of only 15° to 30°F below the NDT temperature. This case clearly emphasizes that at temperatures below the NDT, the presence of localized high residual stresses may trigger the brittle fracture of remarkably thick sections of metal from remarkably small starting cracks, provided propagation stresses are in excess of 5 to 8 ksi levels.

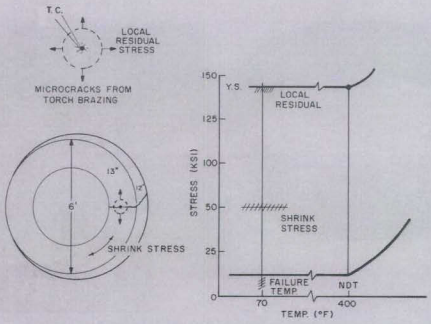

Fig. 44 – (Case B7) Fracture analysis relating to the spontaneous fracture of the ASTM A293 retaining ring forging

Case B8: Forged Turbine Generator-Retaining Ring, SAE 3335 Steel

Composition (Wt – %)						
C	Mn	Si	P	S	Ni	Cr
0.35	0.54	0.15	0.010	0.025	3.39	1.08

Y.S. (ksi)	T.S. (ksi)	El. (%)	R.A. (%)
99.0	122.0	17.7	50.7

NDT (°F)	C_vNDT (ft-lb)	FT (°F)	C_vFT (ft-lb)
180	9	120	5

This failure item represents a forging of old manufacture that had served as a turbine generator retaining ring for 40 years. The bursting of the ring on an overspeed run caused considerable damage, as illustrated by Fig. 45. The dimensions of the ring are illustrated in Fig. 46.

The primary fracture of the ring was traced to a keyway that had been subjected to heavy electrical arcing, resulting from the deterioration of the electrical insulation at this point. The conditions of failure are analogous to those of Case B7. The heavy arcing caused local melting and overheating, resulting in the development of arc crater cracks and high local residual stresses. The required fracture initiation conditions were thus developed after 40 years of service! The general hoop stress of approximately 50 ksi, which represented the service loading of the ring, provided for propagation of the fracture across the 2-1/2 × 16-in. section of the SAE 3335 forging.

The very high (180°F) NDT temperature of the steel was deduced to result from improper heat treatment (by today's standards) for this composition. Laboratory investigations (12) disclosed that the material had been temper embrittled as the result of slow cooling following the quench and tempering heat treatment.

The fracture analysis diagram (Fig. 46) presents a summary of the principal elements of the failure. The service temperature at the time of failure was 60°F below the NDT temperature of the steel. The initiation conditions are represented by yield point levels of stress initiation, and the propagation conditions by the 50-ksi service stress level. The high local stress and small cracks combination had not existed during the 40-year service life of the ring, accounting for the satisfactory performance to the time of the failure of the electrical insulation.

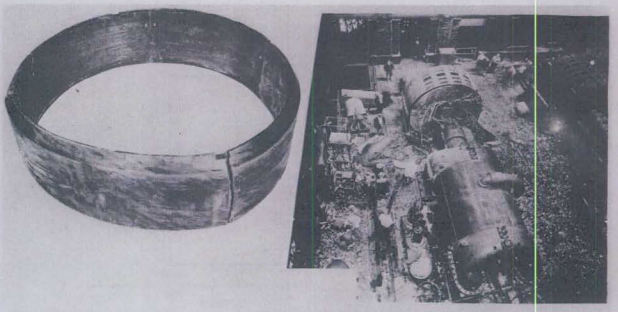

Fig. 45 – (Case B8) Turbine generator failure resulting from the fracture of a 53-in.-diameter retaining ring

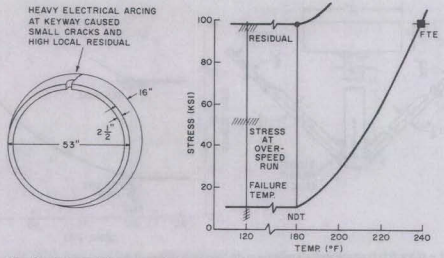

Fig. 46 – (Case B8) Fracture analysis relating to the overspeed run failure of the SAE 3335 retaining ring forging. Data by Greenberg (12).

Case B9: Power Dam Outlet Pipe Manifold, ASTM A201, Grade B Steel

Composition (Wt – %)				
C	Mn	Si	P	S
0.15	0.58	0.20	0.009	0.029

Y.S. (ksi)	T.S. (ksi)	El. (%)	R.A. (%)
28.0	56.0	31.8	55.1

NDT (°F)	C_vNDT (ft-lb)	FT (°F)	C_vFT (ft-lb)
50	7	50	7

This case involved a large (26-ft-diam. by 38-ft-long by 1-1/4-in.-thick) steel outlet pipe manifold for a new hydroelectric power dam. The outlet manifold and piping system had been prefabricated in four parts, which were thermally stress relieved before shipment to the construction site. The four parts were field-assembled with butt welds which were not stress relieved. Prior to final connection into the penstock manifold and piping system, a series of hydrostatic tests were conducted at relatively low pressures. Following these tests, the outlet manifold was emptied to permit several weld repairs and modifications of the internal bracing materials in the outlet manifold. No stress relief was conducted on these field weld repairs. During a subsequent hydrostatic test, a fracture developed (at 155 psig) in the outlet manifold while the pressure was slowly being increased toward 165 psig (1-1/2 times the 110 psig design pressure). The general size and configuration of the outlet manifold and piping system is shown in Fig. 47, top; the extent of damage is shown in Fig. 47, bottom.

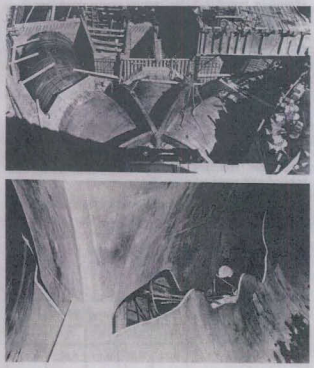

Fig. 47 – Arrangement of hydroelectric power dam outlet manifold and piping system prior to time of failure (top) and extent of fracture in outlet manifold (bottom).

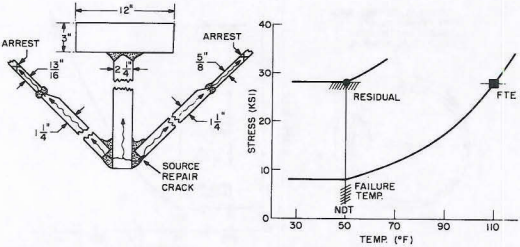

Fig. 48 – (Case B9) Fracture analysis relating to the hydrotest failure of the power dam outlet pipe manifold

The origin of the fracture was a small (1/2 by 1/8-in.) weld-repair crack which extended into the A201-B shell plate at the weld joint connection with the web plate of the reinforcing crotch girder. Fabrication details of this junction weld and the location of the fracture origin are indicated by the drawing of Fig. 48, left. It should be noted that the fracture propagated into three members of the assembly. No data are available, however, for the 2-1/4-in. crotch girder web member because it was repair welded and utilized with new shell plates in the repaired outlet manifold. Fracture arrests resulted after the fractures had run short distances into the 5/8- and 13/16-in. shell plates. As illustrated by the fracture analysis diagram, Fig. 48, right, the failure temperature (50°F) was equivalent to the NDT temperature of the fracture source plate. The initiation stress conditions are indicated to be of the yield point magnitude resulting from the combination of the applied and residual stress fields.

In contrast with the propagation characteristics described previously for the Case C5 failure, the material properties of the A201 plates in which this failure was arrested are particularly revealing. The following data are of primary interest:

Fracture Plates	Thickness (in.)	Composition (Wt – %)				
		C	Mn	Si	P	S
Through	1-1/4	0.21	0.37	0.26	0.012	0.027
End	13/16	0.15	0.55	0.21	0.021	0.034
End	5/8	0.21	0.42	0.28	0.012	0.029

Fracture Plates	Thickness (in.)	Y.S. (ksi)	T.S. (ksi)	El. (%)	R.A. (%)
Through	1-1/4	25.0	56.3	31.5	52.5
End	13/16	32.9	62.0	32.8	62.0
End	5/8	37.2	67.0	32.0	58.5

Fracture Plates	Thickness (in.)	NDT (°F)	C_vNDT (ft-lb)	FT (°F)	C_vFT (ft-lb)
Through	1-1/4	80	7	50	5
End	13/16	20	16	50	28
End	5/8	30	16	50	24

It should be noted that propagation at 50°F through the other 1-1/4-in. plate, which comprised the weld junction with the crotch girder, should be expected because of the NDT temperature (80°F) displayed by that plate. Especially significant, however, is the fact that propagation of this fracture was arrested at both ends upon entering plates of NDT + 20°F and NDT + 30°F quality for the failure temperature (50°F) involved. The nominal stress levels at the fracture end positions were estimated to be slightly below 1/2 the yield strength of both plates in which the failure was terminated. For such stress levels, fracture arrest at NDT + 20°F or NDT + 30°F is in accord with the experimental data of Fig. 12, which served as the basis for the location of the CAT curve in the generalized fracture analysis diagram. The data presented in Fig. 12 indicate a positive assurance of fracture arrest at temperatures of NDT + 30°F and higher; also, there is a high expectancy of fracture arrest for temperatures equivalent to NDT + 20°F.

Category C: Temperature Below NDT – Elastic Stress Loading of Large Flaws

Case C1: Extrusion Press Hydraulic Cylinder, ASTM A27, Grade 70–36 Cast Steel

Composition (Wt–%)				
C	Mn	Si	P	S
0.27	0.67	0.35	0.035	0.027

Y.S. (ksi)	T.S. (ksi)	El. (%)	R.A. (%)
30.7	69.0	27.5	39.0

NDT (°F)	C_vNDT (ft-lb)	FT (°F)	C_vFT (ft-lb)
90	13	70	8

The failure by splitting along one side of a hydraulic cylinder of an 80-ton extrusion press is illustrated in Fig. 49. The fracture originated from a large fatigue crack and propagated through the 13-1/2-in. wall as indicated by the crosshatched region of the drawing. Details of the huge, 16-1/2-in.-long fatigue crack may be noted from Fig. 50. The origins of the fatigue crack may be traced to the presence of a casting shrinkage defect near the inside wall surface. The casting was purchased to ASTM-A27, Grade 70-36 specifications, which involve a conventional casting grade steel, aluminum deoxidized and heat treated by normalizing.

The large, 4400-ton-ram-pressure extrusion press was used intermittently, usually for two or three days, and then allowed to remain idle for several days. Following a three-day idle period, the press cylinder fractured on the first extrusion. The temperature of the cylinder and oil was 70°F at the time of fracture. Prior to this time, repeated extrusions from cold startup had been made successfully. Obviously, the fatigue crack had not yet grown to a sufficient size to initiate fracture at the 13-ksi shell stress – 16-1/2 in. proved to be the critical size!

The fracture analysis diagram of Fig. 49 indicates that the failure occurred at approximately 20°F below the NDT temperature of the steel. The flaw size of 1-1/3 ft is in excellent agreement with the predictions of the generalized fracture analysis diagram of Fig. 9.

Case C2: Extrusion Press Hydraulic Cylinder, ASTM A27, Grade 70-36 Cast Steel

This case, also illustrated by the fracture analysis diagram of Fig. 49, represents failure by leakage of a companion extrusion press hydraulic cylinder. The same extrusion plant also operated a smaller, 2750-ton-ram-pressure extrusion press of 8-1/2-in. wall thickness. The operation of this press was continuous over a 3-year period. The warm oil maintained the shell temperature closely to 120°F during this period.

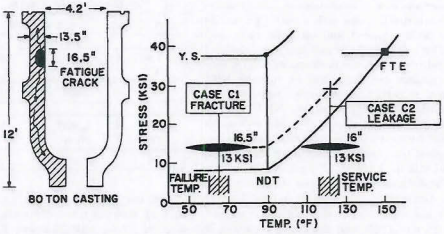

Fig. 49 – (Case C1) Fracture analysis relating to the service failure below the NDT of an ASTM A27 cast-steel extrusion press cylinder. (Case C2) Fracture analysis relating to leakage failure above the CAT of a similar cylinder for a smaller press operating at a higher service temperature.

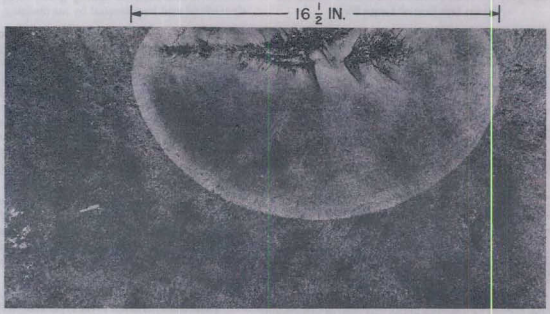

Fig. 50 – (Case C1) Fracture surface of the extrusion press cylinder at the position of fracture initiation from a 16-1/2-in. fatigue crack. Note the casting defect which served as the initiation point for the fatigue crack.

The design stress was 13 ksi, which is conventional for such presses. The cylinder wall of the Case C2 press developed a fatigue crack which penetrated the cylinder wall (approximately 16 in. internal length at the position of penetration). The fatigue crack which caused leakage in this cylinder was at approximately the same position as that which initiated fracture in the Case C1 press. The cylinder was weld repaired and returned to normal operation. The same grade of cast steel was specified for the second press. Data on thickness effects for low-strength normalized cast steels indicate that the NDT temperature of an 8-1/2-in.-thick section may be expected to approximate *but not exceed* the 90°F NDT temperature of the 13-1/2-in.-thick section. Thus, it is reasonable to assume that the same fracture analysis diagram represents the highest temperature position for the Case C2 cylinder, and that the location of the 13-ksi 16-in. flaw point is to the right of the crack arrest curve as plotted in Fig. 49. Accordingly, the conditions for fracture initiation are not attainable for this material at the service temperature of 120°F and stresses in the order of 13 ksi. The stress required for fracture initiation from the 16-in. fatigue flaw (*i.e.*, at the time of leakage) is estimated by the + point to be in the order of twice the level of the operating stress.

Case C3: High-Pressure Air Flask ASTM A372, Class IV Steel

Composition (Wt–%)					
C	Mn	Si	P	S	Mo
0.43	1.59	0.25	0.020	0.003	0.22

Y.S. (ksi)	T.S. (ksi)	El. (%)	R.A. (%)
83.0	116.9	19.0	49.3

NDT (°F)	C_vNDT (ft-lb)	FT (°F)	C_vFT (ft-lb)
90	19	80	17

This case involves a high-pressure compressed air flask of seamless tube construction. The flask dimensions of 1.5-in. wall thickness, 22.5-in. diameter, and 15-ft length represent a large-scale version of a conventional thin-walled pressure bottle used for compressed gases. Fragmentation fracture of the flask occurred during a routine air-leak test conducted at 80°F. The

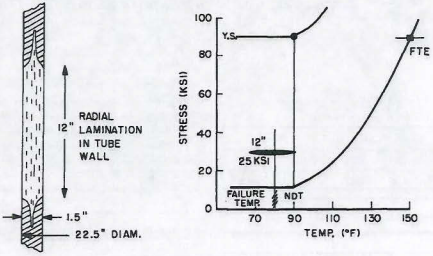

Fig. 51 – (Case C3) Fracture analysis relating to the air-leak test failure of an ASTM A372-IV high pressure air flask

initiating flaw was determined to be a through-the-thickness radial lamination of longitudinal orientation, *i.e.*, following the direction of the primary flow lines resulting from a draw bench forming operation. The through-the-thickness portion of the lamination was approximately 12 in. long, as shown in Fig. 51; a narrow tail-region that extended along the center of the wall was also noted.

The flask successfully resisted fracture for two previous hydrotests of 5-minute durations, and for a "short" period of time in a routine test for air leaks when fragmentation occurred at a pressure which corresponded to a shell stress of 25 ksi. It is believed that the laminated region gradually developed an interconnecting network of "decohesion" regions during these times. When these merged into a network of 12-in. length, the required critical flaw size was attained and fracture resulted. The flask was purchased to ASTM A372-IV specifications.

The fracture analysis diagram (Fig. 51) illustrates that the failure occurred at 10°F below the NDT temperature. The flaw size and stress levels conditions are in excellent agreement with the predictions of the generalized fracture analysis diagram.

Case C4: Turbine Spindle Forging, ASTM A293 Steel

Composition (Wt – %)					
C	Mn	Si	Ni	Mo	Cr
0.30	0.70	0.20	3.0	0.50	0.50

Y.S. (ksi)	T.S. (ksi)	El. (%)	R.A. (%)
85.0	111.0	19.0	50.8

The results of the failure of a large turbine spindle are illustrated in Fig. 52. A detailed account of conditions relating to this failure have been presented by Emmert (13). The failure originated at the core of a massive spindle forging which was 7 ft in diameter and 4 ft long in the central region, as illustrated in Fig. 53. Numerous magnetic particle indications of flakes and thermal cracks were found in the broken sections of the core. The larger of these flaws were noted to be in the range of 6 to 12 in. The failure of the spindle during a routine overspeed test resulted in the fragmentation of the heavy core section into four "quadrant" sections, *i.e.*, pieces in the order of 4 × 3 × 5 ft in size. The failure

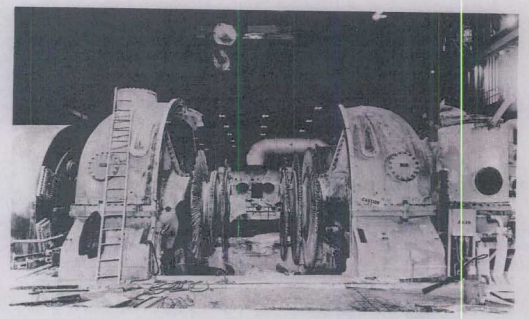

Fig. 52 — (Case C4) Remains of a turbine spindle following fracture and ejection of the 7-ft-diameter center section

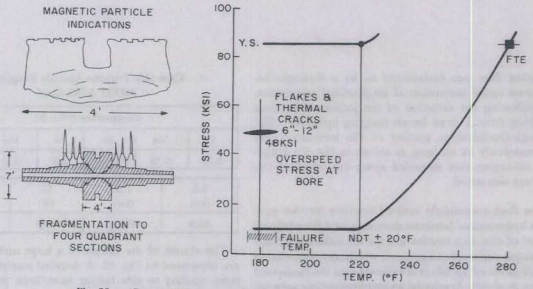

Fig. 53 — (Case C4) Fracture analysis relating to the overspeed failure of the ASTM A293 turbine spindle forging

temperature was determined to be 180° ± 20°F. Charpy V correlation with the NDT tests from the shaft extension section were used to estimate the NDT temperature of the massive core section from Charpy data reported for the massive section. The Charpy data indicated that the NDT of the core section was in the range 220° ± 20°F.

The spindle was purchased to ASTM A293 specification, which is conventional for heavy forgings. The failure temperature, flaw size, and stress conditions established for this failure are in excellent correspondence with the predictions provided by the fracture analysis diagram.

Category D: Temperature Between NDT and CAT Curve – Elastic Stress Loading of Large Flaws

Case D1: High-Pressure Gas Flask, ASTM A302 Grade B Steel

Composition (Wt – %)					
C	Mn	Si	P	S	Mo
0.24	1.33	0.26	0.015	0.014	0.57

Y.S. (ksi)	T.S. (ksi)	El. (%)	R.A. (%)
80.6	104.1	22.0	56.0

NDT (°F)	C_vNDT (ft-lb)	FT (°F)	C_vFT (ft-lb)
30	34	45	40

This case relates to a thick-wall flask used for the containment of high-pressure gases. The failure of the flask, due to the presence of a large lamination, occurred during hydrotest on reaching the specified stress of 57 ksi. The general appearance of the failed flask is shown in Fig. 54; details of the construction and of the initiating flaw are indicated in Fig. 55. The 10-ft-long flask was constructed by welding of 30-in.-O.D. cylindrical forgings of 3.3-in.-wall thickness. High-quality fabrication procedures were used because of the critical application involved in the use of this flask. Exacting x-ray inspection was used during fabrication and following a final stress relief heat treatment. However, the 12-in.-long radial lamination which was the source of fracture was not detected. This is not surprising because of the difficulty of detecting tightly bound lamination defects by nondestructive methods. It should be noted that the lamination defect was entirely contained in the cylindrical forging. The forgings were purchased to ASTM A302-B specifications.

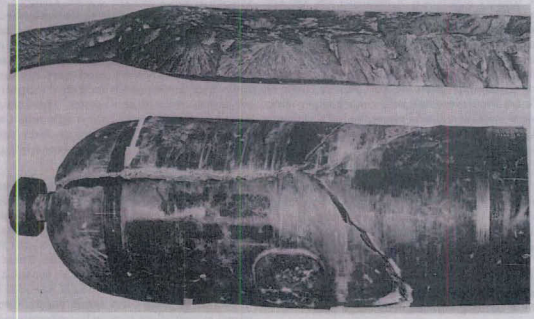

Fig. 54 – (Case D1) Hydrotest fracture of a 30-in.-diameter high-pressure gas flask; the 12-in. lamination flaw origin is shown at the top

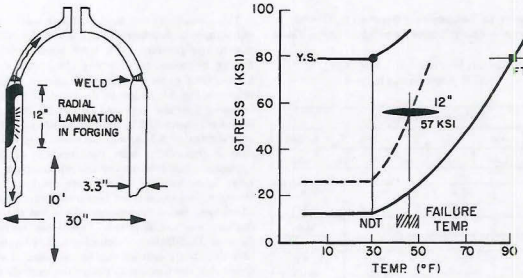

Fig. 55 — (Case D1) Fracture analysis relating to the hydrotest failure of the ASTM A302-B gas flask

The fact that the lamination flaw of almost the exact size of the Case C3 air flask failure required approximately twice the level of stress (57 ksi compared to 25 ksi) for fracture initiation is of particular interest. For the Case D1 gas flask, the failure temperature was approximately 15°F above the NDT temperature, while for the Case C3 air flask, the failure temperature was 10°F below the NDT temperature. The fracture stress for a flaw of 12-in. size would be expected to have the general relationship given by the dashed curve of Fig. 55; *i.e.*, for a given flaw size, a much larger stress is required to cause initiation above the NDT temperature as compared to that below the NDT temperature.

The appearance of the two fractures immediately reflect the conditions of fracture below and above the NDT. The Case C3 air flask vessel fragmented into a large number of small pieces; no shear lips were present on the fracture surfaces. The fracture of the Case D1 gas flask was limited to a few large pieces; shear lips of 1/16 to 1/8 in. thickness were readily visible.

Category E: Temperature at FTE — Plastic Strain Loading of Moderately Large Flaws

The fracture diagram indicates a requirement for combined conditions of plastic overload and large flaws for fracture initiation at temperatures 60°F above the NDT temperature. Excellent confirmation of this requirement have been provided by the results of a series of full-size pressure vessel tests conducted by the Southwest Research Institute for the Pressure Vessel Research Council (PVRC) and the Atomic Energy Commission (14,15). The tests, which were planned by the Low Cycle Fatigue Subcommittee of the PVRC, were intended to evaluate the low cycle fatigue characteristics of various nozzle designs. The growth of fatigue cracks at the nozzles in the course of the tests provided flaw size-fracture stress data for the steels used in the construction of the pressure vessels and nozzles. The unusually high shell stress levels used in these tests reflect a requirement for developing plastic strain level loads in the nozzle regions for the purposes of conducting low cycle fatigue studies.

The tests were conducted at 60° to 70°F using slow, cyclic loading by hydrostatic pressurization. Four vessels were involved; two of these were constructed of ASTM A201 plate with A105 nozzle forgings, and the other two vessels were constructed of ASTM A302-B plate with A182-F1 (modified) nozzles. These materials also conformed to the specifications for steels intended for low temperature service, ASTM A300-58. The NDT temperatures of shell and nozzle materials were determined by postfailure tests, to be uniformly in the range 0° to 10°F except for one component which had a 20°F NDT. Thus, all of the tests which were conducted may be considered as representing tests within 10°F of the FTE temperature which represents the CAT for stress levels equal to the yield strengths of the metals.

Case E1: Fracture of PVRC #1 Vessel

Material	Composition (Wt – %)				
	C	Mn	Si	P	S
A201 Shell	0.18	0.65	0.21	0.010	0.024
A105 Nozzle	0.25	0.72	0.22	0.007	0.034

Material	Y.S. (ksi)	T.S. (ksi)	El. (%)	R.A. (%)
A201 Shell	48.0	67.9	40.0	54.6
A105 Nozzle	36.4	66.6	34.4	50.5

Material	NDT (°F)	C_vNDT (ft-lb)	FT (°F)	C_vFT (ft-lb)
A201 Shell	0	26	60/70	63/72
A105 Nozzle	10	13	60/70	25/30

The general features of all test vessels are illustrated by the failure photograph (Fig. 56) of the first vessel of the test series, PVRC #1. The vessel was constructed from 2-in.-thick ASTM A201 plate and ASTM A105 nozzle forgings. The materials were aluminum deoxidized and heat treated by normalizing. The vessel was subjected to slow, cyclic, hydraulic pressurization to shell stress levels approximating the 48-ksi yield strength of the shell material. Strain gage measurement indicated that the nozzle was loaded plastically to 0.47% strain, resulting in the growth of a low cycle fatigue crack which penetrated the nozzle to a depth of approximately 1-1/2 in. (4-in.-long flaw), at which point (6800 cycles) the test was discontinued and the crack was weld repaired. Continuation of the test resulted in the development of a new crack at the bottom of the weld repair (16) to approximately a 3-in. depth (6-in.-long flaw), at which point (7516 cycles) a brittle fracture was initiated in the nozzle and propagated through the shell (Fig. 57). The fracture surfaces through the shell showed 1/8-in. shear lips. The NDT of the nozzle steel was 10°F and that of the shell 0°F.

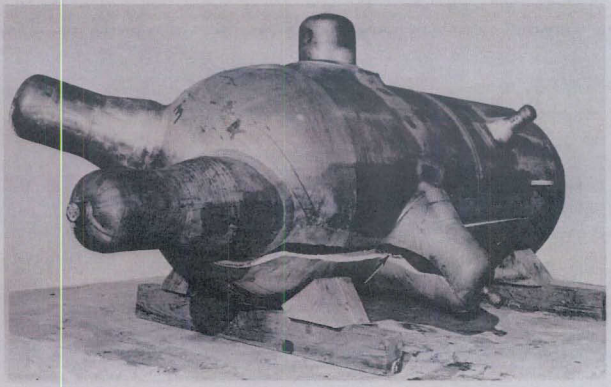

Fig. 56 – (Case E1) Failure of the 3-ft-diameter, low cycle fatigue test vessel PVRC #1. The arrow indicates the location of the 6-in. fatigue crack which initiated the fracture.

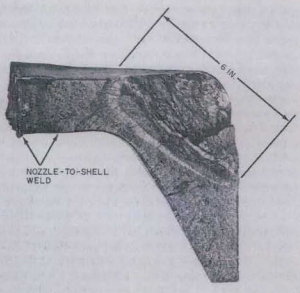

Fig. 57 — (Case E1) PVRC #1 vessel fracture surface illustrating the 6-in. fatigue crack at the nozzle source point (located by the arrow in Fig. 54).

The fracture analysis diagram (Fig. 58) predicts that at the service temperatures equivalent to the FTE temperature of the steel, a large flaw and high plastic load stresses would be required for fracture initiation. Evidently, the 4-in.-long crack which developed during the prerepair portion of the test was not of sufficient size to trigger the fracture. The growth of the second fatigue crack to a length of 6 in. provided the necessary flaw size for fracture. The 6-in. flaw size is in good agreement with the flaw size estimates provided by the general fracture analysis diagram, as indicated by the dashed line of Fig. 58. The 1/8-in. shear lip shown by the fracture surfaces is characteristic of fractures that propagate at FTE temperature, through stress fields at the yield-point-level.

Case E2: Leakage Failure of PVRC #2 Vessel

A second vessel, PVRC #2, which was a duplicate of PVRC #1, was fabricated at the same time, using materials from the same heats of steels (Case E1 properties given above). The Case E2 vessel was cycled at a shell stress of 3/4 the yield strength of the A201 shell material with a resulting nozzle stress of 0.28% strain. Following a discussion of the PVRC #1 failure, the authors recommended to the PVRC Committee that the first fatigue crack which would develop in a nozzle of the PVRC #2 not be weld repaired, as an attempt to continue the testing and develop fatigue crack initiation at other nozzles. It was predicted that the vessel would

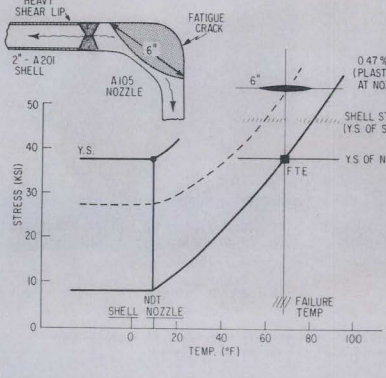

Fig. 58 — (Case E1) Fracture analysis relating to the failure of the PVRC #1 vessel which originated from a 6-in. fatigue crack in a forged ASTM A105 nozzle

not be "lost" by fracture and that the test would be terminated by leakage. Additional testing could then be conducted by removing the failed nozzle and rewelding with a port closure. As predicted, a fatigue crack (7-3/4 in. long, 4-1/2 in. deep) developed which penetrated the nozzle wall (85,868 cycles) and resulted in a failure by leakage. The fracture analysis diagram of Fig. 58 was the basis of the prediction that lowering the nozzle stress level from 0.47% strain to 0.28% strain should result in a requirement for a fracture initiation flaw that is considerably larger than the 6-in. flaw which had almost penetrated the nozzle in the PVRC #1 vessel. As an estimate, the required flaw size should be in the order of 1 to 2 ft. It is evident that the growth of such a large flaw, for the illustrated nozzle configuration (Fig. 57) would result in penetration through the wall prior to fracture. This case provides an excellent example of the use of the fracture diagrams for the prediction of service failure conditions.

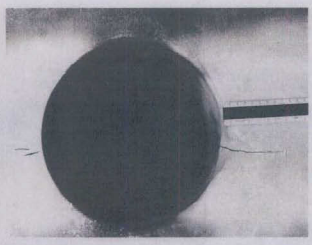

Fig. 59 – (Case E2) Surface appearance of the fatigue crack (right) which penetrated the nozzle wall and resulted in leakage termination of the fatigue test for the PVRC #3 vessel

Case E3: Leakage Failure of PVRC #3 Vessel

Material	Composition (Wt – %)					
	C	Mn	Si	P	S	Mo
A302 – B Shell	0.23	1.23	0.29	0.019	0.021	0.59
A182 – F1 Nozzle	0.22	1.33	0.23	0.011	0.030	0.54

Material	Y.S. (ksi)	T.S. (ksi)	El. (%)	R.A. (%)
A302 – B Shell	60.7	81.3	39.0	64.0
A182 – F1 Nozzle	52.3	74.3	31.0	64.8

Material	NDT (°F)	C_v NDT (ft-lb)	FT (°F)	C_v FT (ft-lb)
A302 – B Shell	20	19	60/70	29/33
A182 – F1 Nozzle	10	16	60/70	30/35

A third vessel, PVRC #3, was constructed of ASTM A302-B shell material and modified A182-F1 nozzle material. Both types of steel were aluminum deoxidized and heat treated by normalizing. This vessel was cycled at a shell stress of 42 ksi with resulting 0.43% plastic strain at the nozzle. Fatigue crack leakage was observed at 8500 cycles. The surface appearance of the crack at the nozzle port opening is illustrated in Fig. 59; the crack appearance is typical of all of the fatigue cracks cited for the PVRC series. The internal appearance of the fatigue crack is shown in Fig. 60. The pad

Fig. 60 – (Case E3) Nozzle section shown in Fig. 57 was cooled with liquid nitrogen and split open in the plane of the fatigue crack (dark region at top left of the fracture surface)

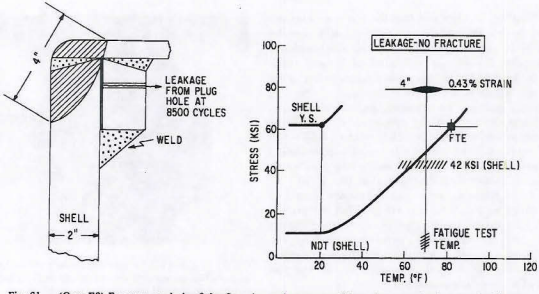

Fig. 61 – (Case E3) Fracture analysis of the flaw size and stress conditions that were inadequate for fracture initiation in the A182-F1 forged nozzle of the PVRC #3 pressure vessel

type nozzle involved in the leakage, featured a plug hole through the pad which provided for leakage at the time that the crack had propagated through to the shell-to-pad interface. The nozzle design and path of leakage are detailed by the drawing in Fig. 61, which also includes the fracture analysis diagram. The high level of fracture toughness of the shell steel at a temperature of 10°F below the FTE is clearly indicated by the resistance to fracture in the presence of a 4-in. flaw subjected to plastic loads of 0.43% strain.

Case E4: Leakage Failure of PVRC #4 Vessel

Material	Composition (Wt – %)					
	C	Mn	Si	P	S	Mo
A302 – B Shell	0.20	1.42	0.19	0.018	0.022	0.52
A182 – F1 Nozzle	0.24	1.35	0.28	0.019	0.017	0.52

Material	Y.S. (ksi)	T.S. (ksi)	El. (%)	R.A. (%)
A302 – B Shell	58.1	79.5	26.0	54.5
A182 – F1 Nozzle	61.8	86.0	28.3	64.6

Material	NDT (°F)	C_vNDT (ft-lb)	FT (°F)	C_vFT (ft-lb)
A302 – B Shell	10	15	60/70	38/43
A182 – F1 Nozzle	10	20	60/70	40/46

A fourth vessel, which was a duplicate of PVRC #3 was fabricated at the same time, using similar materials for the shell and nozzle. This case of E4 provides a simultaneous evaluation of two flaw sizes at two levels of stress. Figure 62 illustrates the two fatigue cracks that developed; one was located in the nozzle at the port opening and the other at the nozzle to shell junction area. Leakage through the nozzle-to-shell junction area terminated the test at 40,041 cycles. The failure developed at the type nozzle that was of the same design as that which initiated failure for PVRC #1 and #2.

The fracture analysis diagram (Fig. 63) illustrates that the shell stress of PVRC #4 was 32 ksi, the plastic stress at the throat section of the failure nozzle was 0.35% strain and the stress at the nozzle-to-shell junction point was 52 ksi. Neither of these two combinations of flaw and stress (2-7/8-in. flaw and 0.35% strain or, 5-in. flaw and 52-ksi stress) were adequate to initiate fracture at the FTE temperature. It should be noted that the case of the larger flaw involves a simultaneous test of the nozzle and shell due to the fact that the flaw extended into both regions.

Summary of PVRC Test Data

The following summary may be made from the described analyses:

Vessel	Flaw Size (in.)	Stress Level	Result
PVRC #1	6	0.47% strain	fracture
PVRC #3	4	0.43% strain	leakage

Vessel	Flaw Size (in.)	Stress Level	Result
PVRC #4	2-7/8	0.35% strain	leakage at 5-in. flaw
PVRC #2	7-3/4	0.28% strain	leakage
PVRC #4 (nozzle)	5	52 ksi	leakage
PVRC #4 (shell)	5	52 ksi	leakage

These results document a consistent performance pattern which fully confirms the fracture analysis diagram predictions that moderately large flaws and stress levels in the plastic overload range are required to initiate fracture at temperatures of NDT + 50°F to NDT + 60°F. In addition, these tests provide a better definition of the flaw size and stress requirement than the previously available estimates. The increased fracture toughness that results from increasing the temperature by 50° to 60°F above the NDT temperature is most dramatic when compared with the information on the extremely small flaw sizes that may trigger fracture at low levels of applied stress below the NDT temperature, *e.g.*, Category B failures. An interesting comparison may be made also with Case A1, Fig. 21, which involved a small flaw and localized plastic stress loads with the service temperature below NDT.

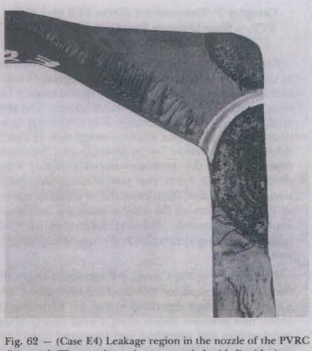

Fig. 62 — (Case E4) Leakage region in the nozzle of the PVRC #4 vessel. The nozzle section was cooled with liquid nitrogen and split open in the plane of the two fatigue cracks (dark areas). The larger of the two fatigue cracks is noted to have penetrated through the thickness of the shell wall. The shiny arc between the cracks is a machine cut to remove a metal fin which covered a portion of the fatigue crack.

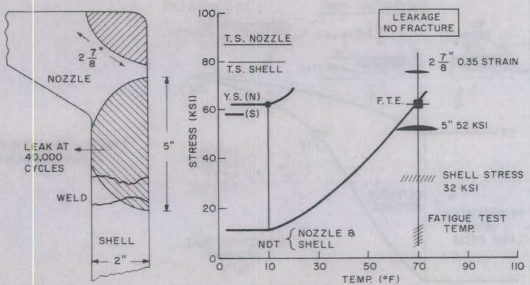

Fig. 63 — (Case E4) Fracture analysis of the flaw size and stress conditions that were inadequate for fracture initiation in the ASTM A182-F1 nozzle and the ASTM A302-B shell of the PVRC #4 vessel

Category F: Temperature Above FTE and Above FTP — Near Ultimate Tensile Strength Loading of Very Large Flaws

Data relating to the subject category were obtained as the result of an extensive series of deliberately flawed and burst tested pressure vessels of approximately 15-ft length × 22-in. O.D. × 1.5-in. wall thickness. The series is of particular interest because it involved test conditions related to various fracture categories. It also involved pressurization by hydrostatic and pneumatic means. In fact, the demonstration of Category F conditions resulted from the pneumatic pressurization tests. Discussions of these cases will be directed not only to documentation of the subject category, but, also at explaining potentially dramatic differences in service failures involving hydrostatic and pneumatic pressurization.

The interest in the Category F test series began with the Case C3 air-leak test failure of the normalized A372 Class IV steel flask described in Fig. 51. Following this event, new pressure vessels using a wide variety of steel compositions and quenched and tempered (Q&T) heat treatments, were manufactured and deliberately flawed for test purposes. These included Q&T A372 Class IV steels, Q&T A336 Class F-22 (2-1/4% Cr, 1.0% Mo) steels, and Q&T HY-80 (3.0% Ni, 1.6% Cr, 0.5% Mo) steels. As a result, the NDT of the test vessels varied from 15°F above the ambient test temperatures (all tests were conducted at 40° to 70°F) to as much as 200°F below the test temperature. All tests were conducted with externally cut "slit" flaws having a sharp root radius of 0.001 in. Two types of slits were used, 10 in. × 0.45T (T relates to the 1.5-in. thickness) and 20 in. × 0.80T. In order to simplify the presentation of these data, the test temperature is represented by the "Δt" between the actual NDT of the vessel and the temperature at the time of test. Thus, a vessel that had a NDT of 200°F below the test temperature is represented as being tested at NDT + 200°F; a vessel that had a NDT of 15°F above the test temperature is represented as being tested at NDT − 15°F, etc. The yield strengths of the vessels varied from 80 to 100 ksi and the tensile strengths from 110 to 130 ksi. For purposes of the diagram summarizations, these have been averaged as approximately 90 ksi and 120 ksi for the yield and tensile strengths, respectively.

Cases F1 to F5: Hydrostatic Burst Tests of Deliberately Flawed Pressure Vessels

Figure 64 presents a summary of the hydrostatic burst tests which involved the use of the 10-in.-long slit. In pressurizing of vessels containing such large slits there is a natural tendency for the slit to open up at the outer surface *i.e.*, to become V-shaped. This condition results

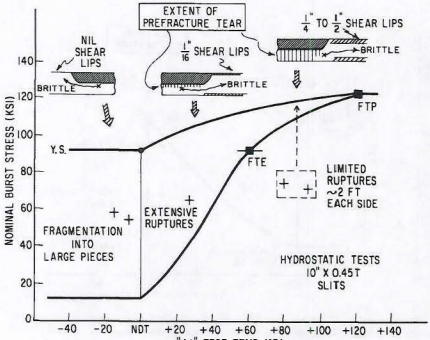

Fig. 64 — (Cases F1 to F5) Summary of hydrostatic burst test data

from the gradual development of an elliptical bulge over the weakened area of the slit. For tests conducted below the NDT the process was terminated *at incipience* by the development of a brittle fracture which originated at the bottom of the above described V. The vessels then fragmented into several pieces (Fig. 65, top). The fracture surfaces were characterized by a lack of visible shear lips, as expected for fractures below the NDT. These events are noted in the diagram of Fig. 64 for the test data points below NDT.

Pressurization at NDT + 30°F resulted in a slightly higher nominal burst stress (according to the formula for thin-walled vessels, PD/2*t*, involving pressure, diameter, and wall thickness) and a distinctly different fracture appearance. The bottom of the V developed a prefracture fibrous tear, and the fracture mode involved very long, branched ruptures rather than several fragments, Fig. 65, center. The fracture surfaces showed a minimum of 1/16-in. thick shear lips which are characteristic of failures at 20° to 50°F above the NDT. A slight bulge had developed prior to fracture because of the increased fracture toughness of the material.

Pressurization at NDT + 80° to + 90°F resulted in an additional small increase in the burst stress and in a dramatic change in the fracture appearance. The fracture which developed stopped approximately 2 ft from each end of the slit, Fig. 65, bottom. Examination of the fracture showed that the prefracture tear had extended completely through the remaining section at the bottom of the V and that a partially brittle fracture had originated from the ends of the slit. The heavy shear lips (1/4 to 1/2 in.) which characterize NDT + 80° to + 90°F temperatures, caused the fracture to propagate at relatively low velocity. As a result, the hydrostatic pressure was lost due to spurting of the liquid and the fracture was arrested after a short run.

The development of a slow, vertical tear through the remaining net section of the slit documents the development of an appreciable bulge prior to fracture. It also documents that for the NDT + 90°F tests, the plotted burst stress conditions (as calculated by PD/2*t*) are fictitious because they do not apply to the bulge area. The actual stresses at the slit ends at the time of fracture initiation in the NDT + 90°F tests are represented in Fig. 64 by the point of the dashed arrow, *i.e.*, close to the ultimate tensile strength of the material.

Cases F6 to F11: Pneumatic Burst Tests of Deliberately Flawed Pressure Vessels

Burst tests of other deliberately flawed vessels featuring test temperatures of NDT + 70°F to + 90°F, NDT + 120°F (at FTP), and NDT + 200°F (above FTP) were conducted with the 20-in. × 0.8T slits and pneumatic loading. Figure 66 presents a summary of the pneumatic burst tests which involved the use of the 20-in.-long slit. Also included in Fig. 66 are the data for the Case C3 air-leak failure, which represents a pneumatic load test below the NDT temperature. The appearance of the Case C3 air-leak test fracture is shown in Fig. 67 (top). The high degree of fragmentation is typical of fractures developed below the NDT temperature for pneumatic pressurization. For hydrostatic pressurization below the NDT temperature, fragmentation with fewer but larger pieces will occur as shown in Fig. 65, top. The other principal difference between the two is that the fragments are projected outward at much higher velocities for the pneumatic case.

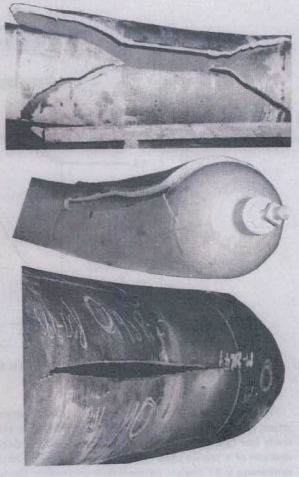

Fig. 65 – Illustrating the general mode of failure of hydrostatically loaded pressure vessels featuring the presence of large flaws. Top – fragmentation into large pieces at temperatures at or below NDT. Middle – extensive ruptures at temperatures of NDT + 30° to NDT + 50°F. Bottom – limited ruptures at temperatures of NDT + 80° to NDT + 90°F.

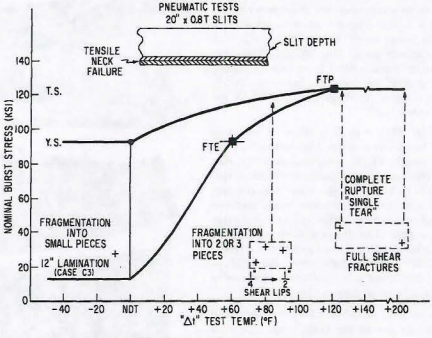

Fig. 66 — (Cases F6 to F11) Summary of pneumatic burst test data

Figure 66 also illustrates that above the NDT temperature, all of the pneumatic loaded vessels failed at relatively low (apparent, PD/2t) burst stresses by the development of a tensile neck failure (to a knife edge) of the remaining 0.2T bridge. Immediately thereafter, the unsupported slit area was bulged severely to an egg shape, as is evident from Fig. 67, bottom. In contrast to the case of hydrostatic pressurization, the pneumatic pressure was not relieved by the escape of a small amount of the pressurizing agent. The high compressibility of the gas provided a continuing "soft spring" loading across the open slit and the resulting tear as it propagated. The tremendous amounts of energy stored in the compressed air not only forced the complete splitting of all pressure vessels of this group, but also acted partially to flatten out the remains. The process is operative even for conditions of fracture by full shear, *i.e.*, above the FTP temperature. The pertinent burst stress levels which are involved for pneumatic burst tests are indicated in Fig. 66 by the heads of the dashed arrows.

The results of these tests may suggest that for extremely large flaw sizes and for conditions of pneumatic pressurization the fracture analysis diagram is irrelevant; such is not the case. Let us consider an analogous case of a flat plate, containing the same flaws and loaded at the same NDT referenced temperatures. The stress levels that would have been required to develop fracture of the plate would have been the same as those developed in the *bulge* regions of the pressure vessels. These are the stress levels indicated in Fig. 66 by the various heads of the dashed arrows. In other words, at FTP the load applied to the plate would have been near ultimate tensile strength levels, as required by the fracture analysis diagram for category F failures near to and above FTP temperatures.

There are several practical lessons to be learned from these tests, over and above the complete corroboration provided for the fracture analysis diagram, as follows:

1. The fracture-safe regions of the diagram, indicated by the temperature zone to the right of the CAT curve, actually represent safety relative to the usual case of spontaneously running fractures (fractures that propagate in the classical brittle fracture sense by release of elastic strain energy from a pre-existing stress field).

2. The unique conditions of local plastic instability (bulge) provide an additional means of fracture propagation which is relatively independent of the general stress field. What is important in this case is the "multi-

plication" of the general stress level which is developed in the partially supported bulge region. Thus, if the flaw is sufficiently large to initiate instability for the level of general (PD/2t) stress, there is no stopping of the tearing action except for a drastic decrease in the general stress level, the reason being that the process basically involves instability—the larger the flaw the larger the bulge and the higher the stress multiplication, etc.

3. It is concluded that for internally pressurized vessels, fracture safety in the region to the right of the CAT curve requires one additional item of consideration—the flaw must not be so large as to provide for the initiation of local plastic instability. Failure to meet this second requirement will result in partial fracture for the hydrostatic case and in total destruction of the vessel for the pneumatic case.

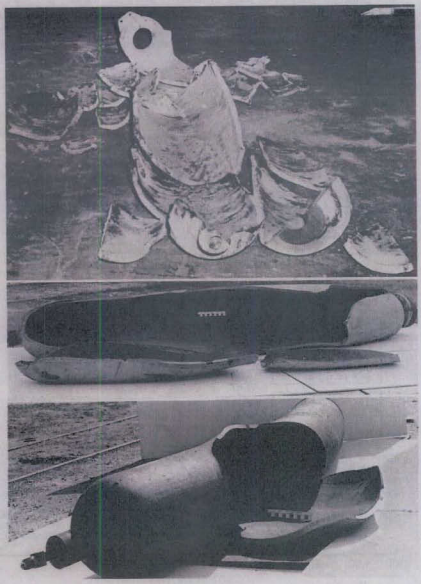

Fig. 67 — Illustrating the general mode of failure of pneumatically loaded pressure vessels featuring the presence of large flaws. Top — fragmentation at temperatures below NDT. Middle—fracture into several large pieces at temperatures of NDT + 80°F. Bottom—ductile tear at temperatures of NDT + 120°F and higher.

GENERAL PROCEDURE FOR THE FRACTURE-SAFE ENGINEERING USE OF STEELS BASED ON THE FRACTURE ANALYSIS DIAGRAM

The foregoing development and explanation of the fracture analysis diagram concepts, with detailed service failure documentation of the validity of the concepts, served the purpose of this final section which considers the interests of the eventual users of the information. We shall now explain the general procedures which have been evolved for the fracture-safe design and engineering specifications of steels based on the fracture analysis diagram.

The principal features of these procedures are illustrated in Fig. 68. It is emphasized that the procedures apply to structures that contain flaws; if it is determined or assumed that the structure is flaw-free there is no need for consideration of the fracture properties of steels! The basic fracture analysis diagram has four primary reference points which may be used as design criteria. These relate to the fabrication and design features of the structure with respect to the use or absence of stress relief, the expected level of stress at critical points (initiation points), the expected size of flaws at initiation points, the general level of stress, considerations of flaw size enlargement consequent to low cycle fatigue, etc. All of these are items requiring engineering design judgment. The four design criteria are defined as follows:

1. *NDT Temperature Design Criterion:* Service use above the NDT temperature is required for structures that are not thermally or mechanically stress relieved or that may be expected to develop points of local yielding, because below the NDT temperature, very small

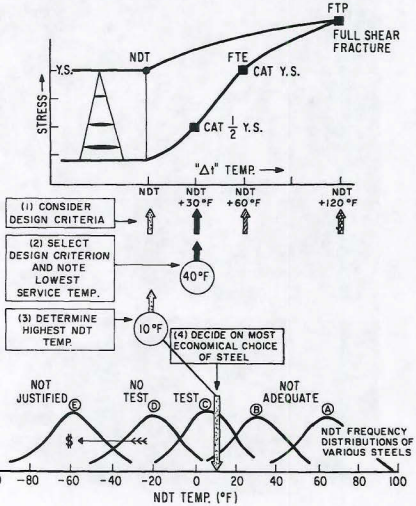

Fig. 68 – An example illustrating the four simple steps for the engineering selection of fracture-safe steels based on the fracture analysis diagram concepts and a catalog of NDT data.

flaws may serve as initiators under these conditions. Fracture protection is afforded by the rapid, stress-axis rise of the initiation curve for small flaws at temperatures above the NDT temperature.

2. *NDT + 30°F Design Criterion:* This design criterion relates to the CAT for stresses in the order of 1/2 the yield strength of the steel. By restricting service use to above this temperature, the flaw-size evaluation problem disappears, provided the level of stress does not exceed 1/2 the yield strength level, as is the usual case. In other words, since the fractures cannot initiate, they cannot propagate. This approach is inherent in the British engineering use of the isothermal Robertson CAT, the Esso use of the CAT for 18 ksi, and all other similar CAT methods.

3. *NDT + 60°F Design Criterion:* This design criterion is based on the same considerations as design criterion 2 above, except that the level of general stress is considered to be equal to the yield strength of the steel. This design criterion applied to the PVRC #1 vessel. It also applies to special cases involving high test pressurization and reactor pressure vessel service conditions at nozzles due to severe thermal stress conditions.

4. *NDT + 120°F Design Criterion:* This design criterion is based on service requirements for plastic overload of the structure, which may either involve considerations of possible accidents or, as in the case of military structures, the expectation of explosive attack. The intent is to restrict service to full shear fracture temperatures in order to develop the utmost of fracture resistance.

Let us assume, for purposes of an example, that engineering judgment dictates the use of the NDT + 30°F (CAT) design criterion, and that 40°F represents the lowest expected service temperature. As noted in Fig. 68, there are four simple steps of the analysis:

1. The four design criteria, as noted on the diagram, are considered in relation to their significance with respect to the specific structure. The choice in this example is assumed to be the NDT + 30°F (CAT) criterion.

2. The lowest service temperature, 40°F for the above stated example, is related to the chosen design criterion.

3. The highest permissible NDT temperature is then determined from the "Δt" scale of the diagram; this is 10°F for the above stated case.

4. The most economical choice of steel is determined by the use of NDT data for the steels of interest, coupled with engineering judgment as to desirability of conducting selection tests as described below.

Let us now assume that information is available as to the NDT frequency distribution curves of steels having the desired strength level and section thickness for the above case. Engineering judgment is then required regarding the most economical selection based on the availability of NDT frequency distribution data as illustrated at the bottom of the figure. The following considerations may apply:

Steels A and B — Not adequate because none of the A steels and only a very small part of the B steel population may be expected to be suitable—test selection is not practical.

Steel C—Approximately 50 percent of the population should be adequate—test selection is required.*

Steel D—All of the population should be adequate and no specification test is required for selection; however, it may be desirable to spot check for quality control reasons.

Steel E—Much lower transition temperature than is required; the added cost over Steel C is not justified.

It should be apparent that the particular requirements of the job will determine the choice between Steels C and D. The question of testing or not testing is a very practical one which relates to costs of purchase on a test requirement basis as compared to the purchase of a more expensive steel that would not require testing.

For other design criteria (NDT, NDT + 60°F, or NDT + 120°F) than the illustrated example, similar procedures as described above are followed.

The authors have engaged in considerable analyses involving the selection of the most economical steels for a wide variety of applications. For such purposes, they have collected a relatively large amount of data involving the NDT frequency distribution curves of various common grades of steel as a function of thickness and heat treatment. Figure 69 presents examples of NDT frequency distribution curves. The top group illustrates the improvement in ship steels which followed the unfortunate experiences of World War II. The curve labeled "World War II" represents the frequency group presented in Fig. 40. The bottom group illustrates high tensile steels of various thickness ranges, as rolled and normalized. This grouping was developed specifically for the selection of fracture-safe steels for a large and

*If it is decided to use the drop-weight test for specification purposes, for the above example, "no-break" performance (1,2) would be required at the specification test temperature of 10°F. This procedure does not require the determination of the NDT temperature; the "no-break" performance indicates that the (accepted) steel has an NDT that is below 10°F.

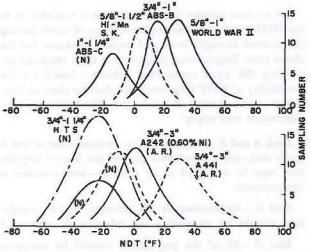

Fig. 69 – Examples of NDT frequency distribution curves taken from the authors' files. The top set relates to ship plate steels. The bottom set relates to high tensile steels of 50 to 55 ksi yield strength.

expensive engineering structure of Navy interest, requiring steels for which such data did not exist. In this case it was necessary to develop NDT distribution curves by random selection of materials. These curves are typically 40° to 60°F wide and approximately 15 to 20 tests based on random sampling serve adequately to define the range. Recourse may also be made to summaries of Charpy V data, provided the correlation index with the NDT temperature is known for the steel.

The appeal of the drop-weight test for developing such frequency bands lies in the fact that it is inexpensive and is quickly conducted. Steels for which the NDT correlation with the Charpy V test has not been established may be tested directly and the necessary data obtained in a few days following the assembly of material selected at random from warehouse and fabricating yard stocks.

The general use of the described procedures is entirely dependent on the knowledge of the NDT properties of steels. Such information is basic to the development of new and improved steels, as well as to the design selection of steels. The information that has been collected by the authors will be provided in a summary NRL Report to follow. It is known that considerable information also exists in the files of various organizations directly interested in the production and use of common grades of steel. It is suggested that pertinent ASTM or ASME committee groups take the lead in cataloging available information and in developing information for "gap" areas. This information may be in the form of NDT data or as Charpy V data which could then be translated to NDT temperatures.

ACKNOWLEDGMENTS

The authors acknowledge the long-range support provided by the management of the Naval Research Laboratory which made it possible to conduct an unfettered program of "brick by brick" development of the subject procedures. Acknowledgment of participating long-range support is also due to BuShips, particularly to Mr. T. J. Griffin of the metals fabrication group. The step by step application of the procedures by BuShips as these were evolved through various rudimentary stages provided invaluable tests of the concepts in practice. Similar expressions of appreciation for application and test of the concepts are due to the engineering staffs of a wide variety of industrial concerns with fracture problems who made available casualty materials and otherwise consulted with and adopted the authors' design recommendations over a period of 10 years.

Finally, an expression of sincere appreciation is due to co-workers, especially for the able assistance in the preparation and conduct of tests, suggestions for the design and construction of equipment, and contributions to the development of standard procedures provided by Messrs. J. Cobb, J. W. Davenport, A. Fox, R. J. Hicks, M. R. Martin, and C. R. McCollum.

REFERENCES

1. Puzak, P. P., and Pellini, W. S., "Standard Method for NRL Drop-Weight Test," NRL Report 5831, Aug. 21, 1962
2. NavShips 250-634-3, "Method for Conducting Drop-Weight Test to Determine Nil-Ductility Transition Temperature of Ferritic Steels," Aug. 21, 1962
3. Irwin, G. R., "Relation of Crack Toughness Measurements to Practical Applications," The Welding Journal 41 (No. 11) 519s – 528s (Nov. 1962)
4. Mosborg, R. J., "An Investigation of Welded Crack Arresters," The Welding Journal 39 (No. 1) 40s to 48s (Jan. 1960)
5. Feely, F. J., Jr., Northup, M. S., Kleppe, S. R., and Gensamer, M., "Studies on the Brittle Failure of Tankage Steel Plates," The Welding Journal 34 (No. 12) 596s to 607s (Dec. 1955)
6. Admiralty Advisory Committee on Structural Steel, "A Comparison of Transition Temperatures Determined by Small and Large Scale Tests on Five Steels," Report No. P2, London: H.M.S.O., 1960

7. Martin, D. C., Ryan, R. S., and Rieppel, P. J., "Evaluation of Weld-Joint Flaws as Reinitiating Points of Brittle Fracture," The Welding Journal **36** (No. 5) 244s to 251s (May 1957)

8. Wells, A. A., "Brittle Fracture Strength of Welded Steel Plates," British Welding Journal **8** 259–277 (May 1961)

9. Hall, W. J., Nordell, W. J., and Munse, W. H., "Studies on Welding Procedures," University of Illinois, Mar. 1, 1962

10. Brandt, F. A., Bishop, H.F., and Pellini, W. S., "Notch Ductility of Type 410 (12% Cr) Stainless Steel," Trans. ASM **48** 368–390 (1956)

11. Babecki, A. J., Puzak, P. P., and Pellini, W. S., "Report of Anomalous 'Brittle' Failures of Heavy Steel Forgings at Elevated Temperatures," ASME Publication, Paper 59-Met-6 (May 1959)

12. Greenberg, H. "How to Distinguish Brittle from Tough Steel," Metal Progress **71** (No. 6) 75–81 (June 1957)

13. Emmert, H. D., "Investigation of Large Steam-Turbine Spindle Failure," Trans. ASME **78** (7) 1547–1565 (Oct. 1956)

14. Lemcoe, M. M. Pickett, A. G., and Whitney, C. L., "Cyclic Pressure Tests of Large Size Pressure Vessels," Progress Reports, Project No. 773–3, Southwest Research Institute

15. Kooistra, L. F., and Lemcoe, M. M., "Low Cycle Fatigue Research on Full-Size Pressure Vessels," The Welding Journal **41** (No 7) 297s to 306s (July 1962)

16. Lange, E. A., and Klier, E. P., "A Study of Fracture Development and Materials Properties in PVRC Vessels 1 and 2," The Welding Journal **41** (No. 2) 53s to 61s (Feb. 1962)

Selected Bibliography Relating to the Development and Applications of the Drop-Weight Test

17. Puzak, P. P., and Pellini, W. S., "Evaluation of the Significance of Charpy Tests for Quenched and Tempered Steels," The Welding Journal **35** (No. 6) 275s (June 1956)

18. Pellini, W. S., "Notch Ductility of Weld Metal," The Welding Journal **35** (No. 5) 217s (May 1956)

19. Pellini, W. S., Brandt, F. A., and Layne, E. E., "Performance of Cast and Rolled Steels in Relation to the Problem of Brittle Fracture," AFS Trans. **61** 243 (1953)

20. Puzak, P. P., Schuster, M. E., and Pellini, W. S., "Crack Starter Tests of Ship Fracture and Project Steels," Appendix entitled, "Procedures for NRL Drop-Weight Test," The Welding Journal **33** (No. 10) 481s (Oct. 1954)

21. Puzak, P. P., and Babecki, A. J., "Normalization Procedures for NRL Drop-Weight Test," The Welding Journal **38** (No. 5) 209s (May 1959)

22. Puzak, P. P., Schuster, M. E., and Pellini, W. S., "Applicability of Charpy Test Data," The Welding Journal **33** 433s (Sept. 1954)

23. Pellini, W. S., and Srawley, J. E., "I. Evaluating Fracture Toughness," pp. 195–198 in "Pressure Vessels for Space, Aerospace, and Hydrospace—A Symposium," Journal of Metals, Mar. 1961

24. Puzak, P. P., Babecki, A. J., and Pellini, W. S., "Correlations of Brittle-Fracture Service Failures with Laboratory Notch-Ductility Tests," The Welding Journal **37** (No. 9) 391s to 410s (Sept. 1958)

25. Pellini, W. S., Steele, L. E., and Hawthorne, J. R., "Analysis of Engineering and Basic Research Aspects of Neutron Embrittlement of Steels," NRL Report 5780, Apr. 17, 1962; also, The Welding Journal **41** (No. 10) 455s (Oct. 1962)

* * *